CHEMISTRY
A European Journal

A Journal of
ChemPubSoc Europe

Accepted Article

Title: A Gold(I) Complex Containing an Oleanolic Acid Derivative as a Potential Anti-ovarian Cancer Agent via Inhibiting TrxR and Activating ROS-mediated ERS

Authors: Wukun Liu, Mianli Bian, Ying Sun, Yuanhao Liu, Zhongren Xu, Rong Fan, and Ziwen Liu

To be cited as: *Chem. Eur. J.* 10.1002/chem.202000045

Link to VoR: http://dx.doi.org/10.1002/chem.202000045

Supported by
ACES

WILEY-VCH

Title

A Gold(I) Complex Containing an Oleanolic Acid Derivative as a Potential Anti-ovarian Cancer Agent via Inhibiting TrxR and Activating ROS-mediated ERS

Authors and affiliations

Mianli Bian,[†[a]] Ying Sun,[†[a]] Yuanhao Liu,[[a]] Zhongren Xu,[[a]] Rong Fan,[[a]] Ziwen Liu,[[a]] and Wukun Liu*[[a,b,c]]

[a] School of Pharmacy, Nanjing University of Chinese Medicine, Nanjing, 210023, P. R. China

[b] State Key Laboratory of Natural Medicines, China Pharmaceutical University, Nanjing, 210009, P. R. China

[c] State Key Laboratory of Coordination Chemistry, Nanjing University, Nanjing, 210023, P. R. China

*Corresponding author. Tel: +86-25-85811633.

E-mail address: liuwukun0000@hotmail.com; liuwukun0000@njucm.edu.cn.

[†] These authors contributed equally to this work.

Notes

The authors declare that they have no conflict of interest.

Abbreviations used

ATF4, activating transcription factor 4; BA, betulinic acid; CDKs, cyclin dependent protein kinase; CHOP, C/EBP homologous protein; CT-DNA, calf thymus DNA; ER, endoplasmic reticulum; ERS, endoplasmic reticulum stress; GA, glycyrrhetic acid; GRP78, glucose-regulated protein 78; IRT, rate of tumor growth; LDH, lactate dehydrogenase; MMP, mitochondrial membrane potential; NAC, *N*-acetylcysteine; OA, oleanolic acid; OC, ovarian cancer; PERK,

pancreatic endoplasmic reticulum kinase; ROS, reactive oxygen species; Sal, salubrinal; TEM, transmission electron microscopy; Trx, thioredoxin; TrxR, thioredoxin reductase; UA, ursolic acid.

Abstract: Many cancer cells critically rely on antioxidant systems for cell survival and are vulnerable to further oxidative impairment triggered by reactive oxygen species (ROS) generating agents. Therefore, the classical design and development of inhibitors that target the antioxidant defense enzymes such as thioredoxin reductase (TrxR) can be a promising anticancer strategy. Here, we show that a gold(I) complex containing an oleanolic acid derivative (**4b**) induces ovarian cancer (OC) A2780 cells apoptosis by activating the endoplasmic reticulum stress (ERS). It can inhibit TrxR enzyme activity to elevate ROS, mediate ERS and mitochondrial dysfunction, finally leading to the A2780 cells cycle arrest and apoptosis. Notably, this complex inhibits A2780 xenograft tumor growth accompanied with increased ERS level and decreased TrxR activity in tumor tissues.

Introduction

Ovarian cancer (OC) is the second most common gynecological malignancies after the cervical cancer, and has the highest mortality rate among gynecological malignancies.[1] Despite recent advancements in OC treatment, including surgical chemotherapy, biological therapy and immunomodulatory, OC remains incurable because of acquired drug resistance and the side effects of intraperitoneal chemotherapy.[2] Due to the short of effective strategy for early screening, most OCs are not detected until advanced stages.[3] Thus, better understanding of molecular mechanisms underlying the growth and metastasis of OC cells is critical for developing novel therapeutic strategies.

Cancer cells generally have higher metabolic demands due to their highly

proliferative nature. The thioredoxin system, including thioredoxin reductase (TrxR), thioredoxin (Trx), and NADPH, regulates cellular signal pathways and proliferation.[4] TrxR is the only known physiological enzyme, which could catalyze oxidized Trx reduction.[5] Many studies have shown that TrxR involved in multifarious physiological and pathological processes, including apoptosis, chronic inflammation and cancer.[6] Significantly, the TrxR is overexpressed in tumors associated with chemoresistance of cancers,[7] TrxR contributes to tumor growth through the hypoxia-inducible factor 1 pathway and plays a crucial role in maintaining cancer phenotype.[8] Increasing evidences show that TrxR is an irreplaceable modulator in tumor development.[9] Therefore, targeting TrxR is a promising way for the OC treatment, however, the upstream mechanism and molecular target are still to be found.

As one of the most important members in the redox control system, the Trx system can be oxidized by abundant reactive oxygen species (ROS).[7a, 10] Cancer cells are exposed to moderate ROS, mainly because of the active metabolism to oncogenic signals.[11] ROS are the byproducts of normal physiological activity, such as the metabolism of mitochondrion and the fold of protein.[12] ROS can activate proliferation and survival pathways at low levels, and cause cell senescence or death at high levels.[12-13] In addition, high level of ROS irreversibly damage DNA and lipids. Recently, the stimulating ROS generation has been an efficacious strategy to target cancer cells.[11]

With the serious intracellular and extracellular stimuli, accompanied by accumulation of ROS, extensive collection of unfolded proteins accumulates in the endoplasmic reticulum (ER).[9] ER, which is mainly to synthesize and fold a great quantity of proteins, along with the intracellular regulation of calcium, lipid synthesis, and transfers to other organelles.[10, 14] The processes make cells unable to maintain ER homeostasis, subsequently, continuous misfolded protein accumulation causes ER stress (ERS) and finally activates the caspase signal cascade resulting in cell apoptosis. However, little attention has

been focused on the complexes with anticancer activities.

Recently, inhibitors targeting the TrxR system have drawn much attention. Among them, a gold-based TrxR inhibitor auranofin exhibits potent antitumor activities and is now even being tested in clinical trials for OC (NCT01747798).[15] Gold complexes have special electronic structures and active unites in redox reactions.[16] They are interacted with reduced biological macromolecules and then exert pharmacological activities.[15b, 16b, 17] Particularly, gold complexes have been covered to trigger antiproliferative effects by interacting the gold atom with sulfur or selenium donor atoms of enzymes such as TrxR.[17-18] However, the sulfhydryl group is necessary for many proteins' function, the off-target interactions with thiols may bring out unexpected side effects for gold complexes.[19] In another way, many gold complexes are ineffective *in vivo* because of their potentiality to exchange ligand with biomolecules, which causes poor activity.

As our sustained curiosity to discover and develop small molecule regulators of cellular redox system as potential therapeutic agents, here we synthesized a series of gold(I) complexes with pentacyclic triterpene (betulinic acid (BA), ursolic acid (UA), glycyrrhetic acid (GA) and oleanolic acid (OA)) derivatives and evaluated for their biological activities. Studies have demonstrated that the pentacyclic triterpene family has different biological functions, such as immunomodulation, anticancer, and antibacterial activities.[20] The antitumor effects of pentacyclic triterpene compounds are characterized by multiple sites, links and targets, which can make the drug exert its efficacy for a long time. Thus, the resulting conjugate of gold(I) complexes with pentacyclic triterpene may exert a different mechanism of action towards cancer cells that can improve safety window of metal-based treatment in malignancy. In addition, we also synthesized a series of cobalt complexes with pentacyclic triterpene derivatives for comparison.

Results and Discussion

10.1002/chem.202000045

Synthesis and Characterization

Alkyne compounds **1a-4a** were synthesized by the corresponding pentacyclic triterpene compounds (BA, UA, GA and OA) and 3-bromopropyne in the presence of potassium carbonate. Then, the same equivalent compounds **1a-4a** and chloro(triphenylphosphine)gold(I) were mixed in THF under the protection of nitrogen to obtain the gold-alkyne complexes **1b-4b** (Scheme 1 and Figure 1A). The cobalt-alkyne complexes **1c-4c** were prepared by the corresponding compounds **1a-4a** and cobalt carbonyl under room temperature (Scheme 2).

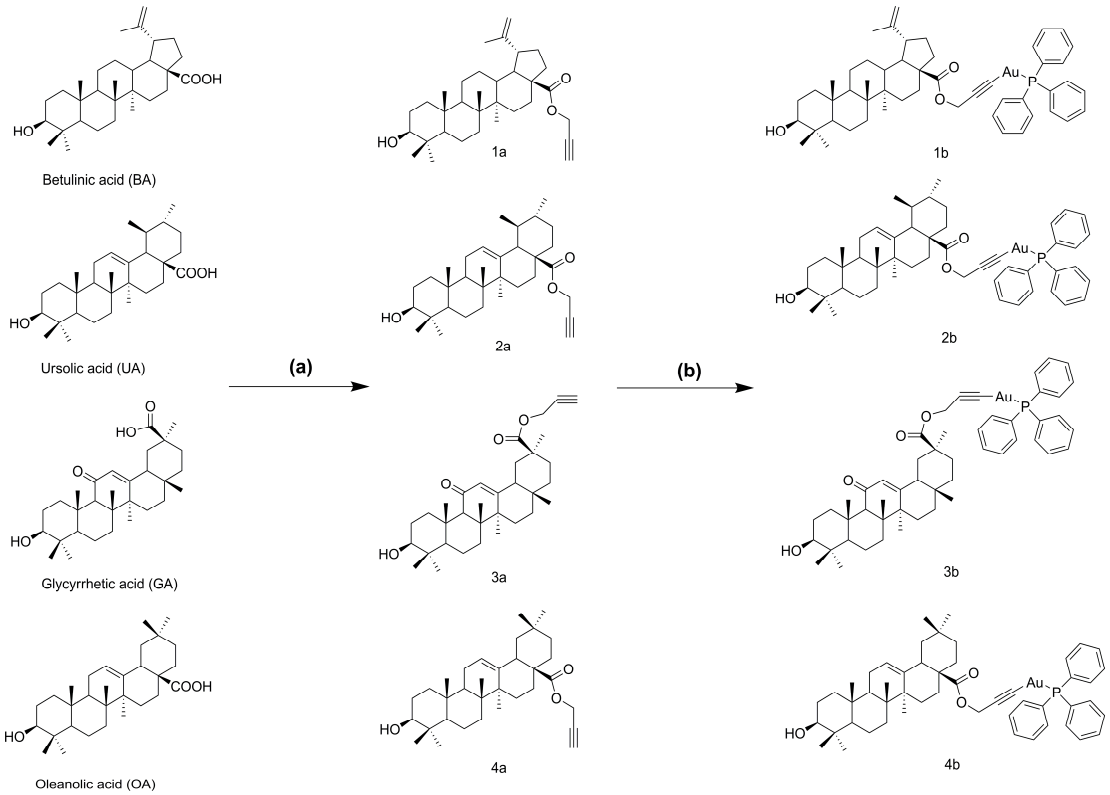

Scheme 1. Synthesis of gold(I)-alkyne complexes **1b-4b**. Reagent and conditions: (a) 3-bromopropyne, K_2CO_3, DMF, 75 °C, 12 h. (b) Cl-Au-PPh_3, NaHMDS, THF, 4 h, N_2.

10.1002/chem.202000045

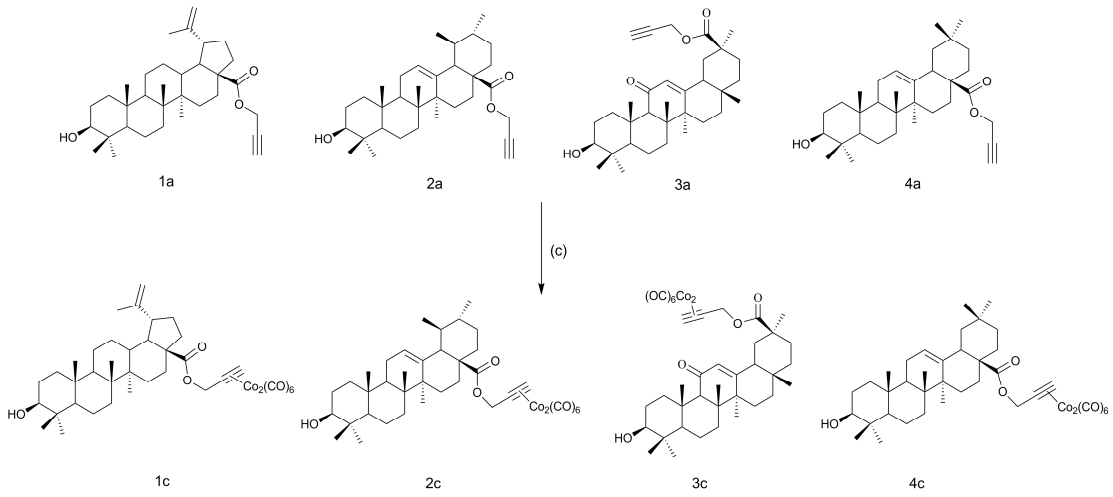

Scheme 2. Synthesis of cobalt-alkyne complexes **1c-4c**. Reagent and conditions: (c) $Co_2(CO)_8$, THF, rt, 16 h.

The structures of **1a-4a**, **1b-4b** and **1c-4c** were verified by NMR and MS spectra. In addition, the purity of gold(I)-alkyne complexes **1b-4b** was determined by elemental analysis. Besides, the stability of the gold complex in the presence of DMSO-d_6/D_2O was tested by examining the ^1H NMR spectra. As expected, **4b** was stable in DMSO-d_6/D_2O (V/V=9:1) at 298 K over 7 days. (Figure S1). There is no obvious change in the ^1H NMR spectra of **4b** within 7 days.

Cytotoxicity in A2780 Cancer Cells

All pentacyclic triterpene compounds (BA, UA, GA and OA), gold(I)-alkyne complexes **1b-4b** and cobalt-alkyne complexes **1c-4c** were tested for antiproliferative activities against breast cancer (MCF-7), colon cancer (HT-29), liver cancer (HepG2) and OC (A2780) cells using the MTT assay. As outlined in Table S1 and Figure 1, gold(I)-alkyne complexes **1b-4b** exhibited lower IC_{50} values in A2780 cancer cells than in other three cancer cells. Particularly, gold(I) complex containing an OA derivative (**4b**) showed the highest cytotoxicity in A2780 cancer cells with an IC_{50} value of 10.24 μM, compared to that of its parent compound OA (IC_{50} = 78.42 μM) and other

10.1002/chem.202000045

compounds. The IC_{50} value of complex **4b** in A2780 cancer cells was similar to that of cisplatin (IC_{50} = 6.49 μM) and auranofin derivative Et_3PAuCl (IC_{50} = 5.74 μM). This complex was 2- to 7- fold higher active against A2780 cells than against HepG2 cells (IC_{50} = 27.11 μM), MCF-7 cells (IC_{50} = 33.26 μM) and HT-29 cells (IC_{50} = 81.75 μM). In contrast, the cobalt-alkyne complexes **1c-4c** were almost inactive in all cell lines (IC_{50} > 100 μM), indicating that the cytotoxicities of complexes depended on the presence of their metal centers. In addition, the lower anticancer activity of OA indicated that the cytotoxicity of **4b** mainly comes from the alkynyl gold(I) PPh_3 scaffold ,which is consistent with Ott's report.[21]

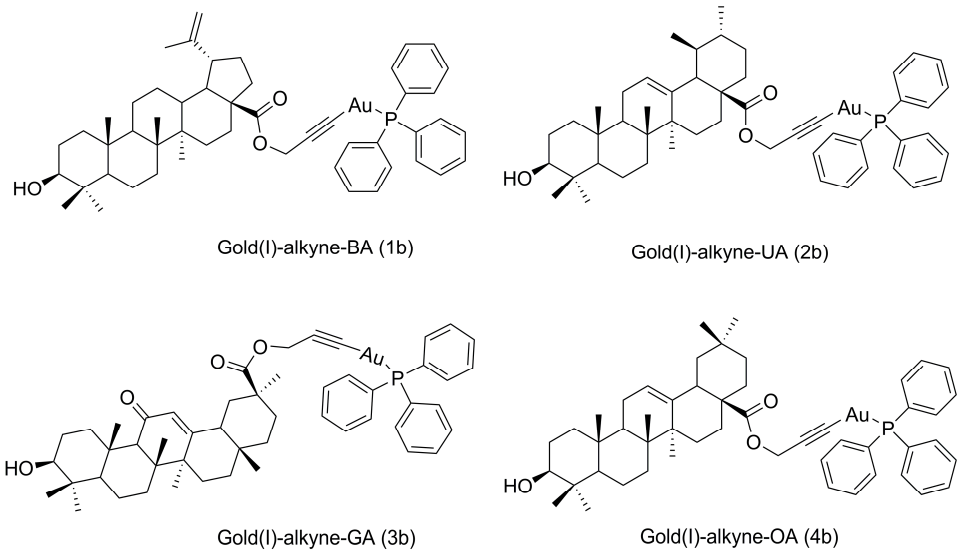

Compound	IC_{50} (μM)	Compound	IC_{50} (μM)
BA	90.74 ± 3.71	1b	25.43 ± 1.71
UA	96.41 ± 2.81	2b	39.63 ± 1.13
GA	80.46 ± 4.13	3b	29.66 ± 1.02
OA	78.42 ± 3.43	4b	10.24 ± 0.21

Figure 1. The structures and cytotoxicity of complexes **1b-4b** in A2780 cells.

10.1002/chem.202000045

Interaction with TrxR

As discussed in the introduction, TrxR has been considered to be the main target of gold complexes. Therefore, we studied the TrxR inhibitory of the most active gold(I) complex **4b,** the corresponding OA and auranofin (as the positive control) on isolated enzyme using DTNB assay. The activity of the purified TrxR was dramatically inhibited by **4b** (IC_{50} = 2.61 μM), which is more potent than the parent compound OA (IC_{50} > 50 μM) (Figure 2A and S2A), suggesting that the TrxR inhibitory effect of **4b** depends on the presence of a gold center. This complex is comparably active as most of gold *N*-heterocyclic carbene complexes but less active than auranofin (IC_{50} of 82.6 nM) (Figure S2B). It should mention that most of gold complexes especially auranofin have potentiality to exchange their ligands with thiol-containing biomolecules before the target enzyme is reached *in vivo*.[22] Besides, compared with the reported natural TrxR inhibitors such as gambogic acid, shikonin and parthenolide,[23] the inhibition of TrxR by gold complex (**4b**) is moderate. Following, we measured the TrxR inhibitory activity of **4b** in cells. Briefly, different concentrations of **4b** were used to dispose of A2780 cells for 24 h and a TrxR assay kit was used to measure the activity of TrxR in cells. In this assay, **4b** showed a TrxR inhibitory activity (with an IC_{50} = 17.45 μM) (Figure 2B). In addition, we identified the influence of **4b** (5 μM, 10 μM, and 15 μM) and OA (100 μM) treatment on the mRNA levels of TrxR in A2780 cells by real-time PCR analysis. As shown in Figure 2C, **4b** dose-dependently reduced the expression of TrxR in A2780 cells. These alterations were further confirmed by immunofluorescence and western blot analysis (Figure 2D and E). The TrxR expression was upregulated in A2780 cells, and the expression was decreased by **4b** in a

10.1002/chem.202000045

dose-dependent manner. Consequently, all these results indicate that TrxR could be a potential target for gold complex **4b**.

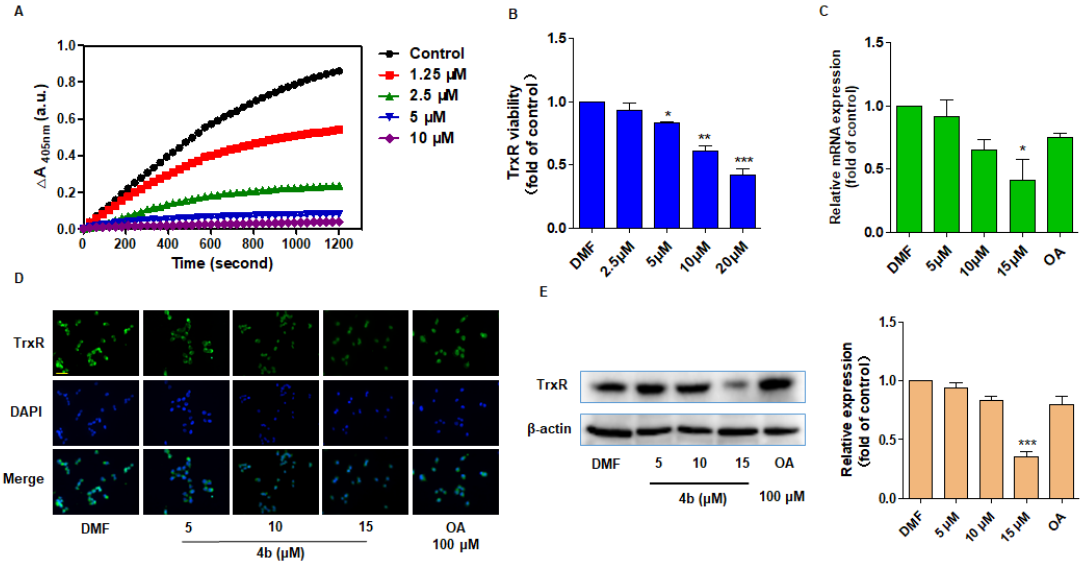

Figure 2. 4b inhibited the expression of TrxR. (A) Inhibition of the purified TrxR by **4b**. (B) Quantification of TrxR activity in A2780 cells treated with **4b** at 37 °C for 24 h. (C) mRNA levels of TrxR in A2780 cells treated with **4b** and OA. (D) Immunofluorescence analysis of TrxR (original magnification, 40×). Scale bars: 25 μm. (E) Western blot analysis of TrxR. Error bars: S.D., n = 3. Statistical significance of differences in mean values: *p < 0.05, **p < 0.01 and ***p < 0.001.

Mitochondrial Dysfunction and ROS Production

Studies have shown that TrxR is a key molecule involved in the intracellular regulation of mitochondrial dysfunction and oxidative stress signaling.[10] Most of gold complexes have been reported to bring out computable mitochondrial dysfunction, and give rise to cancer cell death.[24] Here, we used the JC-1 kit to test the mitochondrial membrane potential (MMP) with the treatment of **4b** (5 μM, 10 μM, and 15 μM) and OA (100 μM). After treated A2780 cells with **4b**, we found that the green (monomeric) fluorescence, which indicates that the MMP is low, was increased compared to the control (DMF) (Figure 3A). This result shows that the mitochondrial dysfunction may be crucial in death

10.1002/chem.202000045

processing induced by **4b**.

Mitochondria are the main sites to produce ROS, and they are vulnerable to ROS attack.[13b] The damage of mitochondria led to the increase of ROS. Thus, A2780 cells were inoculated with **4b** (5 μM, 10 μM, and 15 μM) and OA (100 μM) for 24 h, and fluorescence analysis was used to analyze the production of ROS. As shown in Figure 3B, the imbalanced ROS after treatment with **4b** caused cellular dysfunction consequently.

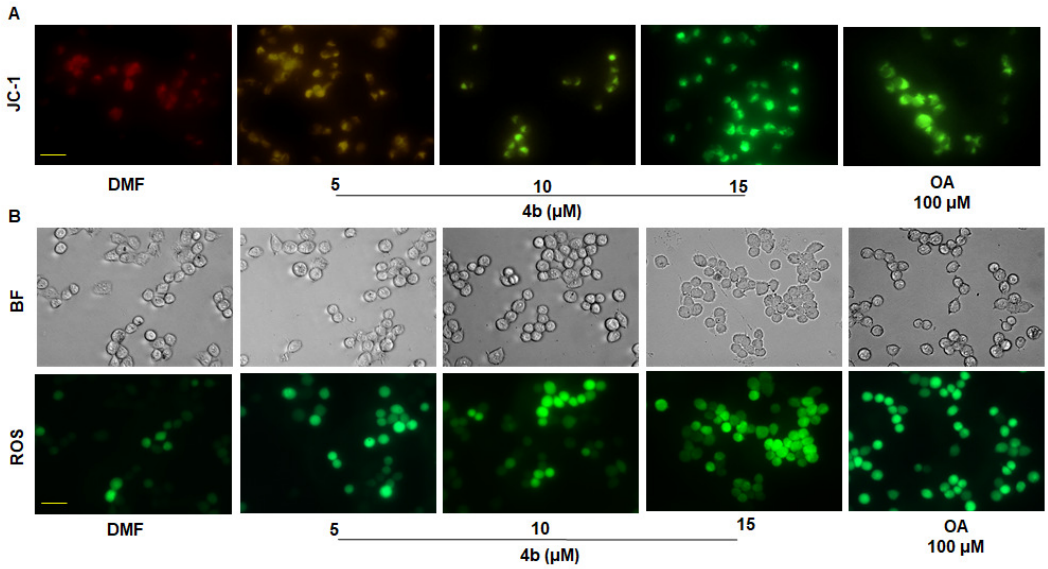

Figure 3. 4b induced mitochondrial dysfunction and ROS production. (A) Mitochondrial membrane damage imaged by JC-1 staining treated with **4b** and OA (original magnification, 40×). (B) Bright-field image and ROS positive cells treated with **4b** and OA (original magnification, 40×). Scale bars: 25 μm.

4b Activated ERS in A2780 Cells

It is worth noting that the death-inducing ability of anticancer compounds has been to do with ROS producing and its capacity to induce ERS.[25] Simultaneously, the presence of ROS and ERS stimulated the presentation of different damage-associated molecular patterns, which can result in cancer cells death in different mechanisms.[26] Based on the mitochondrial depolarization after treatment with **4b**, we tested the

10.1002/chem.202000045

intracellular ROS and ERS in A2780 cells. The level of ROS was detected by 20,7-dichlorodihydrouorescein diacetate (H2DCFDA) which is oxidized to the brightly fluorescent 20,70-dichlorouorescein (DCF) by cellular ROS. And we used ER-Tracker Red to test the ER variation, which can bind to the sulfonylurea receptors on ER and turn to bright red. Using the cell fluorescence microscopy, we noticed a clear colocalization of ROS with the ER after incubating with **4b** (5 μM, 10 μM, 15 μM) and OA (100 μM) for 24 h. The **4b** could activate the colocalization of ROS and ERS dose-dependently, and significantly increase the fluorescence in comparison with the lead compound OA (Figure 4A). The activation of ERS is extremely possible owing to the increased membrane permeability of ER after the drug stimulation.

The findings above urged us to find the interesting pro-apoptotic pathway activated by **4b** in A2780 cells. ERS-induced cancer cell apoptosis becomes a novel signaling target during the development of cancer therapeutic agents.[26-27] After treating A2780 cells with **4b** (5 μM, 10 μM, and 15 μM) for 24 h, C/EBP homologous protein (CHOP) and Calnexin, which are an ER chaperone and a major marker of prolonged ERS respectively, were up-regulated compared with the treatment of OA (100 μM) by immunofluorescence analysis (Figure 4B and C). The expressions of pancreatic endoplasmic reticulum kinase (PERK), activating transcription factor 4 (ATF4) and glucose-regulated protein 78 (GRP78) were all dramatically up-regulated by western blot analysis, indicating the activation of ERS (Figure 4D and E). The persistent activation of ERS leads to the failure of ER functions and cell death, typically through apoptosis. These results indicated that **4b**-induced ROS led to the activation of a lethal ERS, which at least partly contributed to the apoptosis in OC cells.

10.1002/chem.202000045

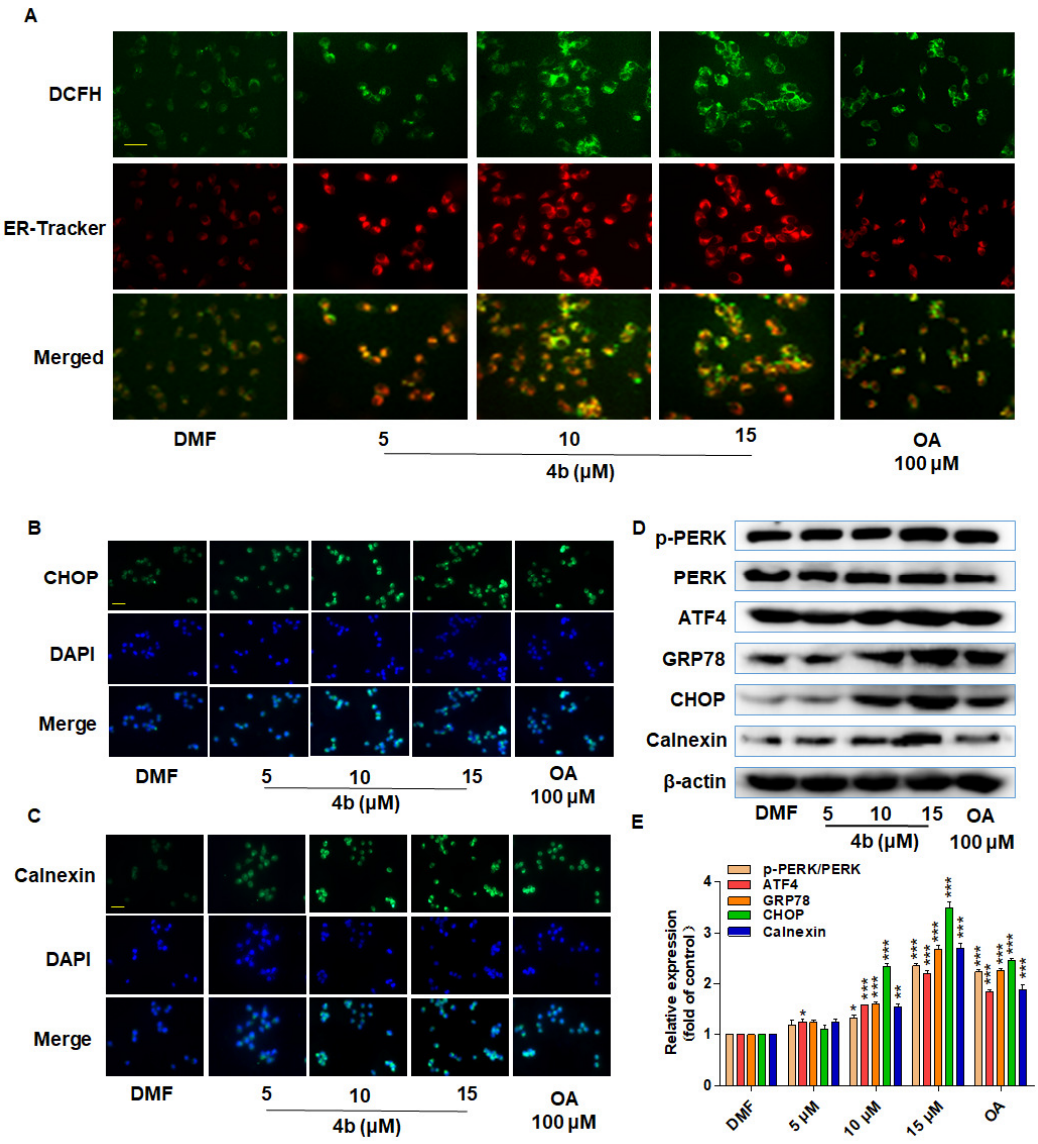

Figure 4. 4b induced the activation of ERS in A2780 cells. (A) Immunofluorescence analysis of cells treated with **4b** and OA for 24 h (original magnification, 40×), and incubation with DCFH (ROS indicator, green) and ER-Tracker red (Red). (B, C) The expression of ERS marker factors (CHOP and Calnexin) by immunofluorescence analysis treated with **4b** and OA for 24 h (original magnification, 40×). Scale bars: 25 μm. (D, E) The expression of ERS-inducing factors by western blot treated with **4b** and OA for 24 h. Statistical significance of differences in mean values: *p < 0.05, **p < 0.01 and ***p < 0.001 (n = 3).

4b-induced Apoptotic Pathways

The interaction of ROS and ERS is an important event in triggering a variety of death-pathways. Particularly, apoptosis is considered to be one of the key

mechanisms resulting from ROS and ERS. So we studied the way **4b** induced the A2780 cells apoptosis. Exposing phosphatidylserine (PS) generally precedes the loss of plasma membrane integrity in apoptosis.[28] Normal cells are unreactive to annexin V-FITC, which is the marker of PS, and propidium iodide (PI) enters cells with disrupted plasma membranes. However, when the cells underwent the stimulation of drugs, they were reactive to annexin V-FITC but remain unreactive to PI.[11, 29] Cells in the late phase of apoptosis and necrotic cells are reactive to both annexin V-FITC and PI. In Figure 5A and B, after treatment with **4b** (5 μM, 10 μM, and 15 μM) and OA (100 μM) for 72 h, the percentage of apoptotic cells was dose-dependently increased with **4b**, and the number of apoptotic cells in **4b** (15 μM) treatment is more than that of the OA group.

Besides ERS, the overexpression of ROS could cause mitochondrial dysfunction, induce the mitochondrial membrane depolarization, provoke cytochrome c release from mitochondria into the cytosol, and ultimately result in other proapoptotic molecules increasing in the cytosol.[30] Bcl-2 family adjusted the mitochondrial membrane permeabilization, which is the main process in programmed cell death. This finding showed that the dysfunction of mitochondrial plays an irreplaceable role in A2780 cells induced by **4b** (5 μM, 10 μM, and 15 μM). In addition, to confirm the induction of the intrinsic pathway, we tested several important proteins expression using western blot. **4b** increased the expression of the pro-apoptosis proteins Bax, AIF and cytochrome c, but it restrained the expression of pro-survival proteins Bcl-2 (Figure 5C and D). The level of apoptotic marker (AIF) by immunofluorescence analysis is consistent with western blot (Figure S3). Together with the obvious morphological characteristics in apoptotic cells, such as cytoplasmic and nuclear condensation, DNA breakage, membrane dysfunction, and loss of microvilli,[31] **4b** (5 μM, 10 μM, and 15 μM) and OA (100 μM) were used to induce nuclear morphology and detect by Hoechst 33258 staining. The cells showed weak blue fluorescence and appeared as regular round contours in

10.1002/chem.202000045

DMF control, and the nuclei of A2780 cells appeared hyper condensed (brightly stained) (Figure 5E). This means that **4b** induces the strong apoptosis in A2780 cells.

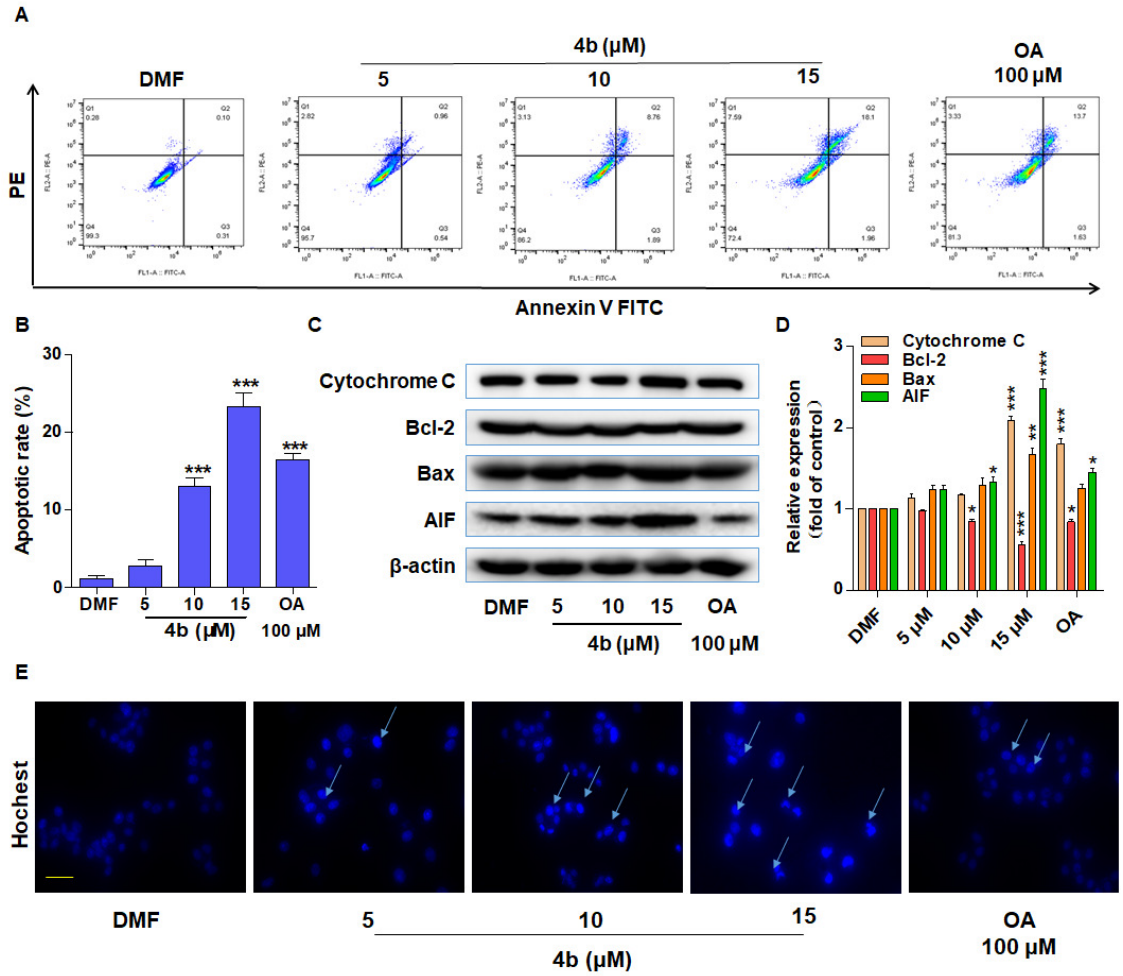

Figure 5. 4b-induced apoptotic pathways. (A, B) Apoptosis of A2780 cells treated with **4b** and OA for 72 h. (C, D) Western blot analysis of A2780 cells treated with **4b** and OA for 24 h. (E) Hoechst 33258 staining treated with **4b** and OA for 24 h in A2780 cells (original magnification, 40×). Scale bars: 25 μm. Error bars: S.D. Statistical significance of differences in mean values: *p < 0.05, **p < 0.01 and ***p < 0.001 (n = 3).

Next, the effect of **4b** (5 μM, 10 μM, and 15 μM) and OA (100 μM) on cell cycle progression was investigated by the PI staining. Cells were treated with **4b** at different concentrations for 72 h, showing that the proportion of cells that accumulated in the S phase increased compared to the G0/G1 and G2/M phases (Figure S4A and B). Based on this result, we further tested the

cycle-related proteins' levels of S phase by western blot analysis (Figure S4C and D). The expression levels of Cyclin A and CDK2 were significantly reduced after treatment of **4b** (15 μM), while the levels with OA treatment was almost unchanged. These results reached a conclusion that ROS accumulation plays a significant role in **4b**'s anti-cancer actions in A2780 cells and also acts as upstream signaling molecules involved in **4b**-induced mitochondrial activation.

4b Activates ROS-dependent ERS, which Contributes to Membrane Interaction and Disruption in OC Cells

Live cell imaging indicates that **4b** impair membrane integrity, which could be detected by lactate dehydrogenase (LDH) assays. So we analyze the leakage of the cytoplasmic enzyme LDH into the culture medium, an indicative index of plasma membrane disintegration. As shown in Figure S5A, **4b** induces LDH release from the A2780 cells in a dose-dependent manner. To explore whether ROS plays an important role in **4b**-induced cytotoxicity and DNA damage, we used *N*-acetylcysteine (NAC), which is the specific ROS inhibitor, to decrease ROS expression in this study. Results indicated that NAC alleviated **4b**-induced cytotoxicity (Figure S5B). Next, we tested and verified the expression of ROS with the treatment of NAC (2 mM) by DCFH dyeing kits, the result indicated that NAC could inhibit the ROS expression and **4b** offset this effect (Figure S5C). This finding indicated that the interactions between the assemblies of **4b** and the cell membrane may lead to cytotoxicity, and the mechanism underlying NAC inhibitor alleviating **4b**-induced cytotoxicity in A2780 cells need be further studied.

Subsequently, we explored whether the ROS accumulation in the ER domain induced the activation of ERS.[32] To confirm the misfolded protein accumulation in ER, **4b** on the morphology in A2780 cells was observed by transmission electron microscopy (TEM). As shown in Figure 6A (in both

10.1002/chem.202000045

×5000 and ×12000 amplification), DMF-treated A2780 cells showed the familiar appearance of smooth ER (arrow). However, treated with **4b** (10 μM) for 24 h, the ER lumen in A2780 cells became swelling (arrow). It means that complex **4b** induced the formation of translucent vacuoles in large quantities, which represented the activation of ERS. It was considered to be the downstream mechanism of ROS to induce the cells apoptosis. Besides, this result is in accordance with Che's report that ER plays an important role in gold complex induced cytotoxicity and ERS is associated with the apoptotic event.[33]

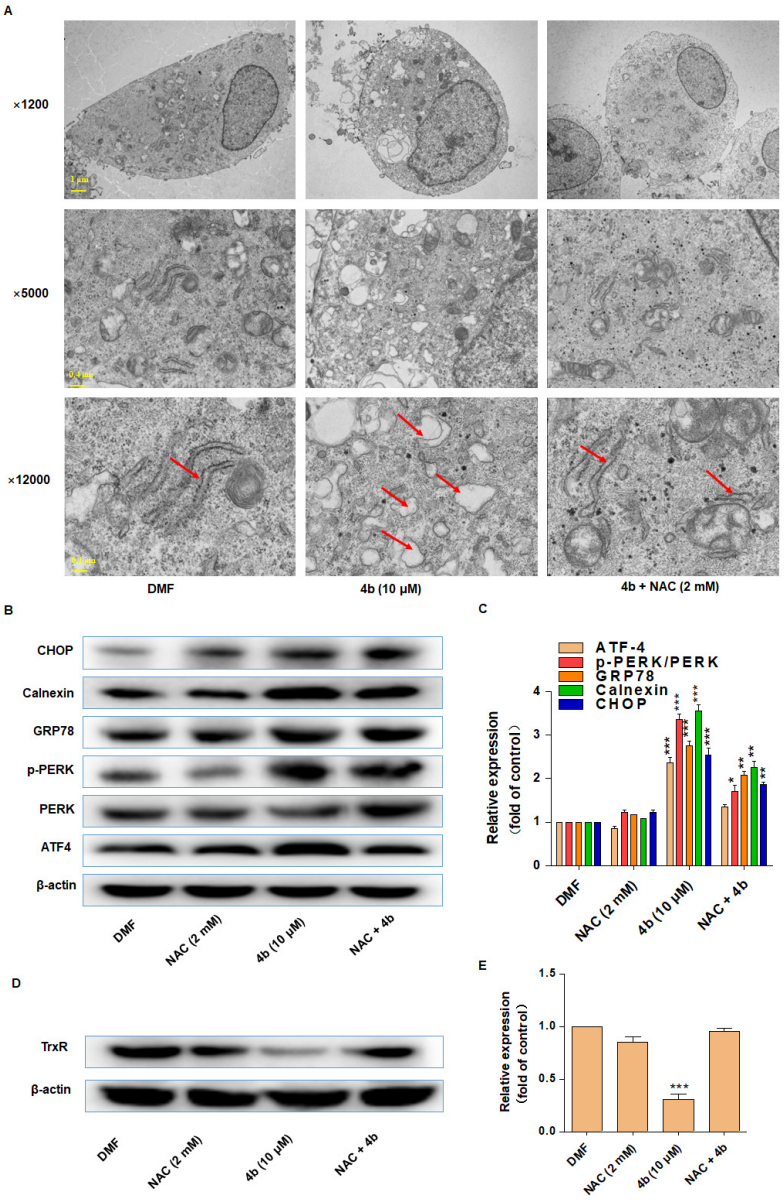

Figure 6. 4b activates ROS-dependent ERS in OC cells. (A) Effect of **4b** and NAC on the morphology of ER in A2780 cells. (B, C) Western blot analysis of A2780 cells treated with **4b** and NAC for 24 h. (D, E) The expression of TrxR by western blot treated with **4b** and NAC for 24 h. Error bars: S.D. Statistical significance of differences in mean values: *p < 0.05, **p < 0.01 and ***p < 0.001 (n = 3).

Interestingly, the ROS inhibitor NAC (2 mM) alleviated **4b**-induced accumulation of misfolded protein in ER. Thus, our observations confirmed the producing of ROS accompanied by the activation of ERS. Treated A2780 cells with specific NAC confers cytoprotection against cell death through ERS. In Figure 6B and C, the markers of ERS were all high expression in **4b** treatment and reversion by NAC. Following, we tested the TrxR expression, the result was the opposite trend when compared with apoptosis indicators (Figure 6D and E). Conjointly, our studies indicated that the biological action of **4b** in A2780 cells is reliant on its interaction with TrxR and ERS.

Activation of ERS is Required for 4b to Induce A2780 Cells Apoptosis

As high ROS levels can trigger mitochondrial membrane, we next tested whether inhibiting ERS protected cells from **4b** inhibited TrxR expression. Cells viability in A2780 showed that although **4b** (10 μM) efficiently reduced the viability of TrxR, salubrinal (Sal) (10 μM) treatment can counteract this effect observably (Figure 7A). Western blot and immunofluorescence analysis are consistent with the results (Figure 7B-D). The Trx system is significant to maintain the intracellular redox balance and prevent the generous accumulation of ROS.[34] The inhibition of TrxR could disturb the redox balance, finally resulting in the intracellular ROS accumulation in cancer cells. Interestingly, the ERS inhibitor Sal can counteract this phenomenon. In Figure 7E, we can know that **4b** (10 μM) promoted the expression of ROS, and the Sal (10 μM) inhibited the expression of ROS. Furthermore, western blot showed that treatment with **4b** (10 μM) dramatically decreased the levels of

10.1002/chem.202000045

anti-apoptotic Bcl-2 but increased the levels of pro-apoptotic Bax expression in A2780 cells. Increasing the Bax/Bcl-2 ratio facilitates cytochrome c release into the cytosol and further activates the caspase cascades.[35] Therefore, we tested the indicator and apoptosis marker (AIF), the result revealed that salubrinal can counteract the **4b** apoptotic effect (Figure 7F). Quantitative analysis revealed the same results (Figure 7G). The expression of apoptosis marker (AIF) by immunofluorescence analysis is consistent with western blot analysis (Figure S6). These findings collectively suggested that **4b** restrained the expression of TrxR, which can be counteracted by the ERS inhibitor Sal.

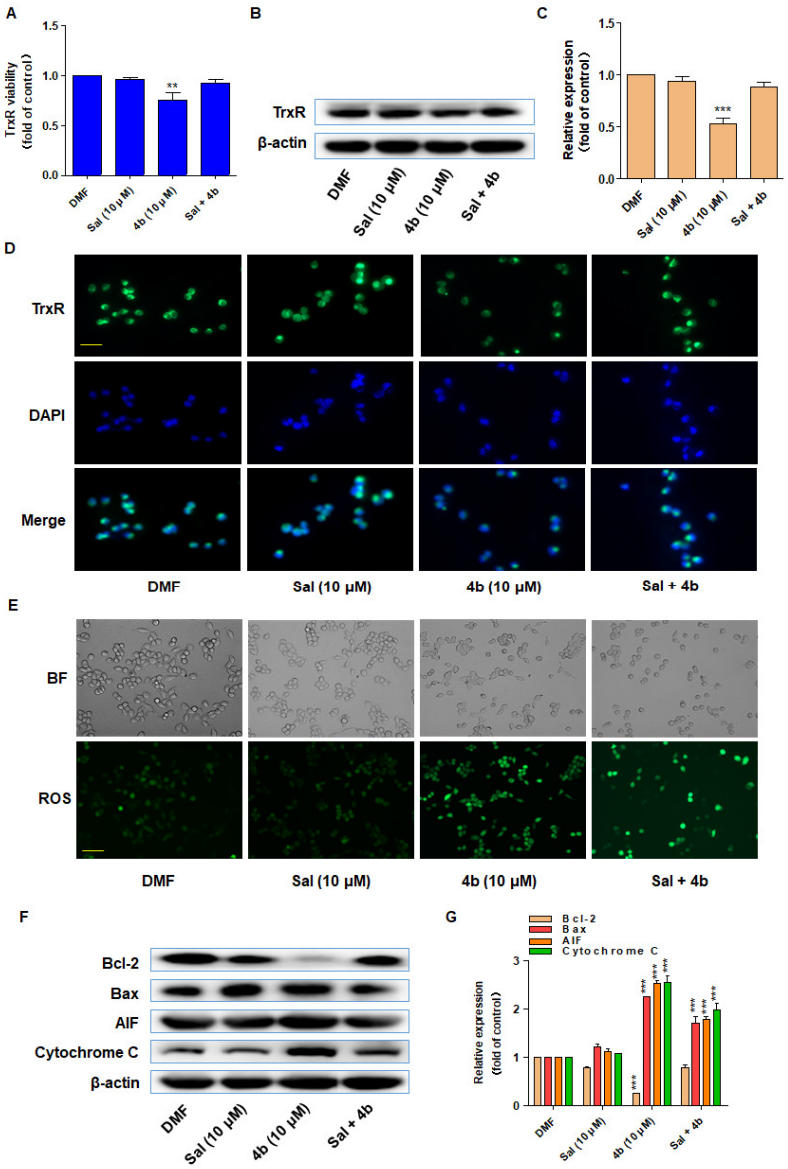

Figure 7. Activation of ERS is required for **4b** to induce A2780 cells apoptosis. (A) Quantification of TrxR activity in A2780 cells treated with **4b** and Sal at 37 °C for 24 h. (B, C) Western blot assays in A2780 cells. (D) Immunofluorescence analysis in A2780 cells (original magnification, 40×). (E) Bright-field image and ROS positive cells treated with **4b** and OA (original magnification, 40×). Scale bars: 25 μm. (F, G) Western blot analysis in A2780 cells treated with **4b** and Sal for 24 h. Error bars: S.D. Statistical significance of differences in mean values: *p < 0.05, **p < 0.01 and ***p < 0.001 (n = 3).

Binding Sites between TrxR and 4b

As the effective inhibition of TrxR by gold complex **4b** was demonstrated, then the binding sites between TrxR and **4b** were analyzed by molecular docking software (Figure 8B). SEC498/CYS497 residues are widely considered as the crucial active sites of TrxR and involved in the interaction of the enzyme with the complexes.[5, 36] In particular, the amino acid SEC498 is always considered as an inhibitor targeting site. Gold complexes are the most effective inhibitors of TrxR, particularly auranofin which was proved to interact with the active site SEC498.[37] Curcumin, a TrxR inhibitor, was found to irreversibly bind with the active sites SEC498/CYS497,[9a] and recently the new analog of curcumin (WZ26) was proved to be an effective TrxR inhibitor and analyzed its binding sites with TrxR (SEC498, CYS497, GLY496, GLN494, LEU493, SER404 LYS123, GLU122, ALA119).[38] After exposing the binding pocket of TrxR in docking procedure, we found that the key residues around **4b** included SEC498, CYS497, GLY496, GLN494, LEU493, and ASP491. Dramatically, the docking graphical results showed that the functional atom gold of **4b** bound with crucial residue SEC498. With regard to the OA group of **4b**, the bulky one binding with the sites named GLN494, LEU493, and ASP491, which may be instrumental for the remaining half of gold ligand binding and anchoring in the pocket of TrxR (Figure 8A). Combined the above experimental data and the docking

10.1002/chem.202000045

results account for **4b**, this complex may have a potential direct binding with TrxR.

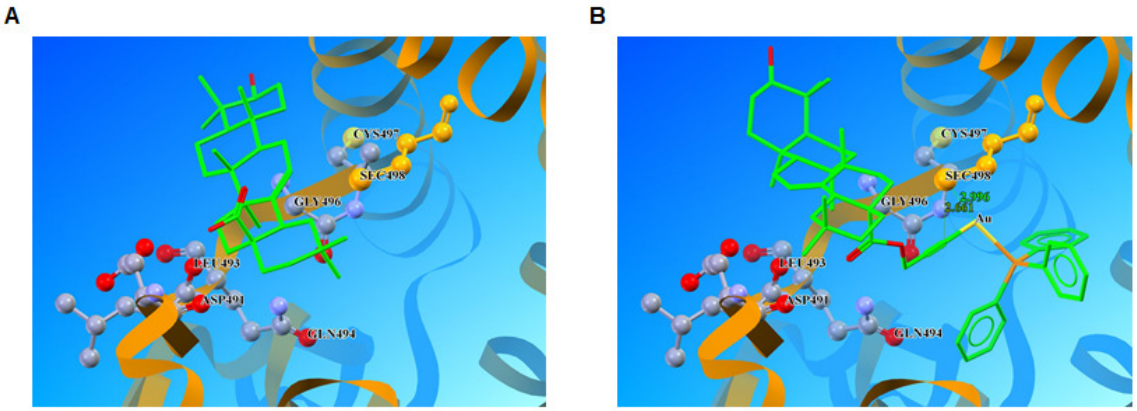

Figure 8. Modeled configuration of inhibitors in the binding sites of TrxR. The binding sites are labelled, and inhibitors are drawn as green sticks. (A) Protein and inhibitor interactions for OA. (B) Protein and inhibitor interactions for **4b**.

Interaction with DNA

It is widely accepted that DNA symbolizes a primary target of anticancer metal complexes and some gold(I) complexes have also been proven to target DNA recently.[17, 39] To more clearly find out the anticancer activity of our complex and to figure out whether there is an interaction between our gold complex and DNA, the DNA binding was studied to identify the binding of **4b** with the calf thymus DNA (CT-DNA). The absorption of the complex **4b** has an obvious hyperchromicity with the DNA concentration increasing during 250-300 nm (Figure S7A). However, the absorption of OA has no significant change, indicating the alkynyl gold(I) PPh_3 scaffold may play a major role in **4b**'s effect (Figure S7B). This result inferred that there may be a hydrogen bonding action between complex **4b** and CT-DNA. Next, DNA conformational changes induced by complex **4b** were investigated by circular dichroism spectroscopy. The interactions of **4b** with CT-DNA were studied in PBS buffer solution (pH = 7.2) at various ratios (r_b = [**4b**] / [DNA] of 0.0, 0.1, 0.5, 1.0, 2.0). The circular

10.1002/chem.202000045

dichroism (CD) spectra of CT-DNA exhibited a negative band at 240 nm due to the helixity of B-DNA and a positive band at 270 nm due to base stacking. As shown in Figure S8, the positive CD signal was significantly reduced at 273 nm. This may indicate π–π interactions between the DNA nucleobases and the π-system of **4b**.

4b Inhibited A2780 Xenograft Tumor Growth Accompanied with Increased ERS Level and Decreased TrxR Activity in Tumor Tissues

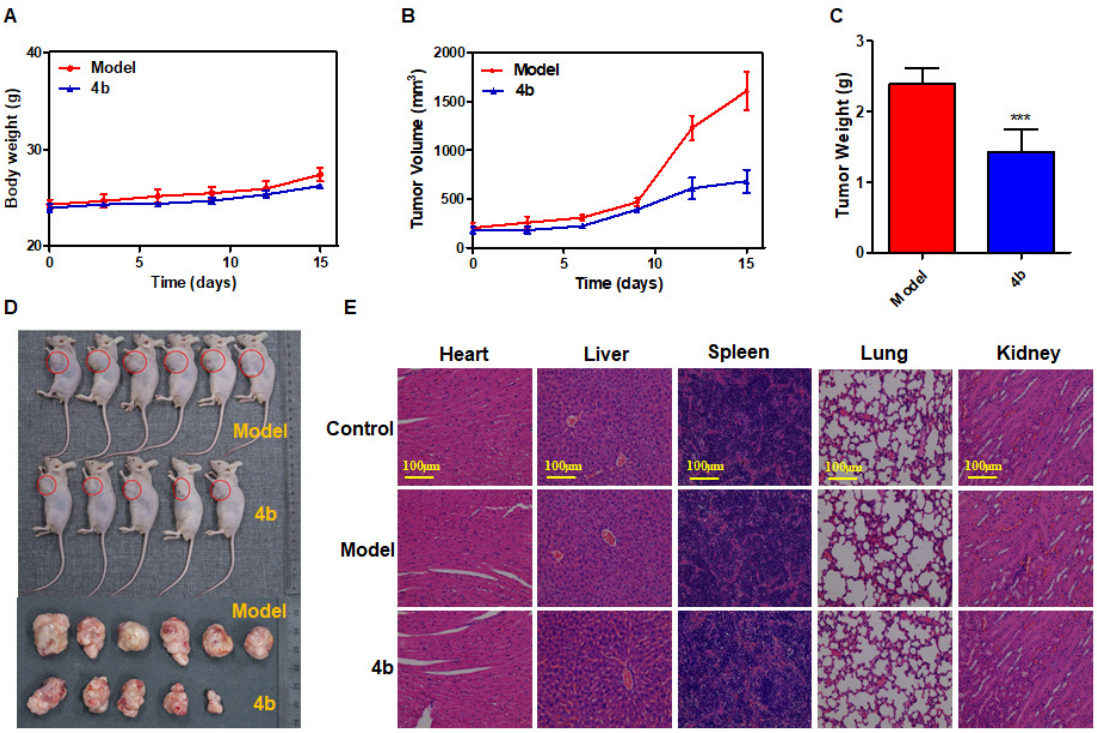

Figure 9. 4b inhibited A2780 xenograft tumor growth. (A) Effect of treatments on the mean body weight of mice. (B, C) **4b** inhibited tumor volume and tumor weight of A2780 human OC xenografts in nude mice. (D) Images of representative tumors. (E) HE staining of the major organs (original magnification, 20×). Values are the mean ± SEM. For the statistics of each panel in this figure, data are expressed as mean ± SD (n = 6); *** P< 0.001 compared with model.

To assess the impact of **4b** *in vivo*, we used a subcutaneous xenograft model of A2780 cells in immune deficient mice. Intraperitoneal administration of **4b** at

10.1002/chem.202000045

doses of 20 mg/kg for 15 days obviously reduced weight and tumor volume versus model. The **4b** treatment group was well tolerated, without clear weight loss (Figure 9A and B). At the end of the study, we collected the tumors, and weighed to calculate the inhibition rate of tumor growth (IRT). **4b** treatment group showed an IRT as high as 40.2% (Figure 9C), the difference can also be seen in the tumor images shown in Figure 9D. H&E staining analysis further indicated nontoxicity in mouse hearts, livers, spleens, lungs and kidneys (Figure 9E). However, the nucleus in tumor tissues were heteromorphic, showing pathological mitosis, focal necrosis and a large number of new blood vessels in tumor tissues (Figure S9).

Furthermore, the activity of TrxR in tumor was measured by the TrxR kit assay, and the result indicated that **4b** treatment group obviously reduced the TrxR activity (Figure 10A). Western blot and immunofluorescence analyses are consistent with the TrxR kit assay (Figure 10B and C). Besides, western blot and immunofluorescence analyses of the tumor tissues revealed that **4b** treatment group could increase the levels of CHOP and AIF, indicating that **4b** induced apoptosis in A2780 cells is accompanied by the activation of ERS (Figure 10D-G). Overall, treatment of **4b** inhibited the tumor growth *in vivo* by down-regulation of TrxR expression.

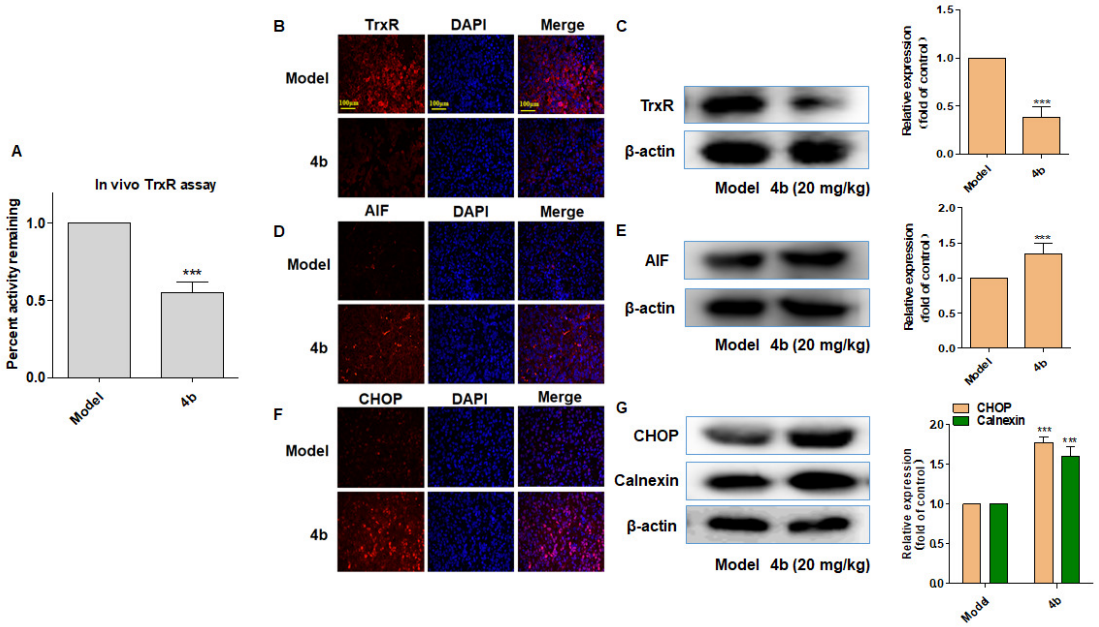

10.1002/chem.202000045

Figure 10. 4b inhibited the TrxR activity in tumor xenografts with the occurrence of apoptosis and ERS activation. (A) TrxR enzyme activity of tumor tissues was measured by TrxR activity detection kit. (B, D, F) Tumor tissues were stained with immunofluorescence using antibodies against TrxR, AIF and CHOP. DAPI to stain the nucleus (original magnification, 40×). Scale bar = 100 μm. (C, E, G) Western blot analysis on the expressions of TrxR, AIF and CHOP cleavage from respective tumor tissue lysates. β-actin was used as protein loading control. For the statistics of each panel in this figure, data are expressed as mean ± SD (n = 6); *** P< 0.001 compared with model.

Conclusion

Numerous antitumor agents have been reported to increase ROS producing in cancer.[40] Different mechanisms have been studied, such as redox cycling and mitochondrial oxidase activation.[4, 41] Our results indicated that the most active gold(I) complex **4b** containing an OA derivative targets TrxR to induce ROS in A2780 cells and activate ROS-dependent ERS activation. Eliminating the ROS by the ROS inhibitor NAC or ERS by the ERS inhibitor salubrinal totally abolished the anticancer effects of **4b** in cells. Combining the *in vivo* experiments, our research provided a molecular mechanism by which **4b** induces ROS-ERS mediated apoptosis in cancer cells, and shed light on understanding how **4b** works *in vivo*.

As shown in scheme (Figure 11), **4b** inhibited TrxR, deteriorated the mitochondrial dysfunction, and preferentially killed OC cells. TrxR has appeared as a significant target in cancer chemotherapy. It related to tumor growth, drug resistance, and insensitive patient prognosis.[42] Therefore, the novel inhibitors of the system, which are developed as potential antitumor agents, have caught the attention in the past few years. Besides, **4b** can induce the expression of ROS and here elaborate its biological functions. Binding of **4b** to TrxR suppresses the physiological functions, which results in the assemblage of ROS, and finally reducing oxidative stress. Excessive accumulation of ROS can cause mitochondrial dysfunction and reduce the MMP.

10.1002/chem.202000045

Our study showed that **4b** obviously depressed the MMP ($\triangle_{\psi m}$) in A2780 cells and NAC completely reversed **4b**-induced mitochondrial dysfunction, pointing out that ROS production is the upstream regulator of mitochondrial dysfunction. These findings highlight that **4b**-induced oxidative stress is related to mitochondrial dysfunction, which might strengthen the lethal effects of **4b** in OC treatment.

By the increasing ROS, treatment of **4b** is accompanied by inducing ERS response, which is stressed by high expression of ERS markers. CHOP induction is probably most sensitive to ERS response, and it is considered as a downstream coactivator marker of ERS-induced apoptosis. In other words, **4b**-induced ERS is a secondary response to **4b**-induced ROS and it could overstate the cell death instead of being a mediator in OC cells. In conclusion, the considerable ROS release and TrxR inhibition of **4b** induced a prominent ERS response. The observation of **4b** sheds fresh light on the possibility of combining with oxidative stress and anticancer treatments.

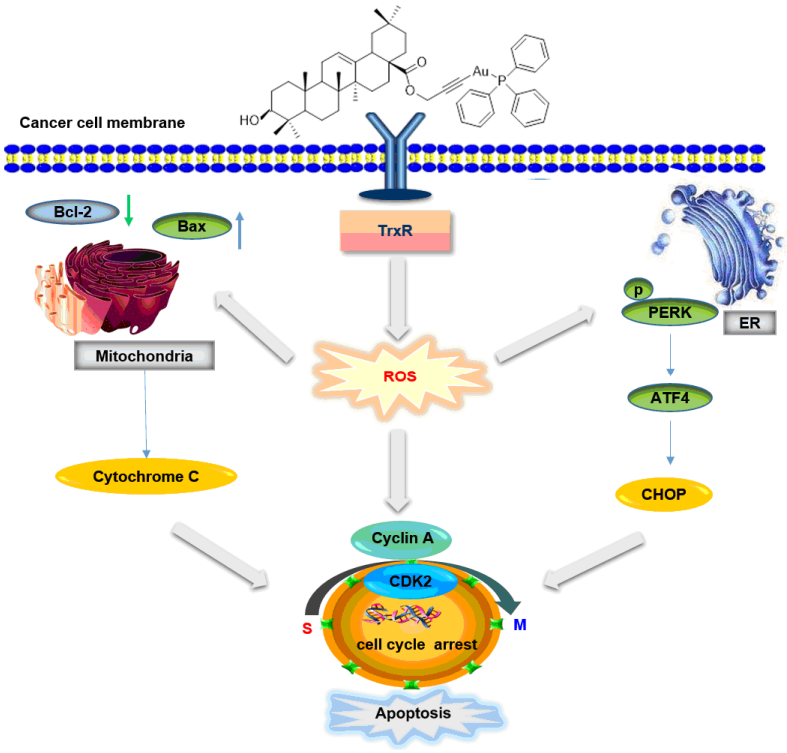

Figure 11. Schematic illustration of **4b** process by targeting TrxR-ROS-ERS.

10.1002/chem.202000045

Materials and Methods

Reagents and Antibodies

All chemicals and spectral grade solvents were obtained commercially and were used without further purification. Solvent was dried and used according to standard procedures. All chemical reactions were monitored by TLC. Deuterated solvents were purchased from Cambridge Isotope Lab Inc. (CIL). Solutions for all spectroscopic and biological studies were prepared with solvents of HPLC grade and doubly distilled water from Millipore (>18.2 MΩ). **4b** dissolved in DMF and the control group was treated with 0.1% DMF. Antibodies, such as Bcl-2, Bax for western blot, were purchased from Abcam Co. (China). AIF was purchased from Wuhan Sevier Biotechnology Co. (China). TrxR and β-actin were purchased from Proteintech (Chicago, USA). JC-1 assay kit was purchased from KeyGen Co. (Jiangsu, China); ROS assay kit, ATP assay kit and all secondary antibodies were purchased from Beyotime Biotechnology (Jiangsu, China). TrxR activity assay kit was purchased from Solarbio. Purified TrxR (rat liver), ATPase activity assay kit and calf-thymus (CT-DNA) were purchased from Sigma-Aldrich Co. (China). Antibodies against Calnexin, CHOP, PERK, and ATF4 were purchased from Wan Lei Biology Antibody (Shenyang, China). The primers used in quantitative real-time polymerase chain reactions (qRT-PCR) were purchased from GenScript Co. Ltd. (Nanjing, China). Phosphate buffered saline (PBS), Dulbecco's Modified Essential Medium (DMEM), fetal bovine serum (FBS) and trypsin-EDTA were bought from GIBCO BRL (Grand Island, NY, USA).

^{1}H and ^{13}C NMR data were acquired on a Bruker AV-500. MestReNova software was used to analyze NMR spectra. Elemental analyses were determined on a PE 2400 Series II. UV-2401PC spectrophotometer was used

for recording electronic absorption spectra. The IR spectra were acquired on Thermo Nicolet iS10. Circular dichroism spectra were recorded on circularly polarized fluorescence spectrometer CPL 300. Fluorescent microscopy was performed using a Leica DMi8 fluorescence microscope. ESI-MS spectra were obtained by Agilent 6125. Flow Cytometer was BD C6 Plus. MTT and protein assays were quantified by Perkin-Elmer Fusion Reader (Packard BioScience Company).

Synthesis and Characterization

All chemical reactions were monitored by TLC. Solvent were dried and used according to standard procedures. All chemicals and spectral grade solvents were obtained commercially and were used without further purification. The purities of the target compounds **1a-4a** and **1b-4b** were confirmed by elemental analysis. And the analyses indicated by the symbols of the elements or functions were within ± 0.5 % of the theoretical values. Complex **4b** was stored in DMSO-d_6/D_2O (V/V = 9:1) at 298 K for 7 days, then assayed by ^{1}H NMR spectroscopy.

The general synthesis of compounds 1a-4a: A 50 mL round bottomed flask was charged with the corresponding pentacyclic triterpene compounds (BA, UA, GA or OA) (0.88 mmol), K_2CO_3 (1.75 mmol) and DMF (15 mL). After stirring well, 3-bromopropyne (1.75 mmol) was added, and the reaction mixture was stirred for 12 h at 75 °C. Then the reaction solution was concentrated in vacuo and the rude residue was further purified by column chromatography (silica gel; PE/EA).

Alkyne compound 1a (PE/EA = 15:1)：Yield: 68%. ^{1}H NMR (500 MHz, Chloroform-d) δ 4.75 – 4.67 (m, 2H, H-32), 4.66 – 4.57 (m, 2H, H-30), 3.18 (dd, *J* = 11.4, 4.8 Hz, 1H, H-2), 3.01 (td, *J* = 11.1, 4.9 Hz, 1H, H-34), 2.43 (t, *J* = 2.5 Hz, 1H), 2.31 – 2.15 (m, 2H), 1.90 (td, *J* = 8.7, 7.9, 5.4 Hz, 2H), 1.68 (s, 5H),

1.64 – 1.47 (m, 3H), 1.48 – 1.30 (m, 7H), 1.30 – 1.20 (m, 2H), 1.20 – 1.13 (m, 1H), 1.12 – 0.99 (m, 1H), 0.96 (d, *J* = 2.1 Hz, 6H), 0.92 (s, 3H), 0.92 – 0.82 (m, 1H), 0.81 (s, 3H), 0.75 (s, 3H), 0.71 – 0.64 (m, 1H). ^{13}C NMR (126 MHz, Chloroform-d) δ 175.18 (C=O), 150.45 (C=C), 109.65 (C=C), 78.99 (C≡C), 77.21 (C-OH), 74.32 (C≡C), 56.60 (C-O-), 55.36, 51.33, 50.58, 49.52, 46.86, 42.41, 40.82, 38.87, 38.73, 38.28, 37.21, 36.80, 34.34, 31.96, 30.52, 29.64, 27.99, 27.42, 25.55, 20.89, 19.39, 18.30, 16.14, 16.02, 15.35, 14.72. ESI-MS: Calcd for $C_{33}H_{50}O_3$, $[M]^+$: 494.38; Found: $[M]^+$: 494.8. Anal. Calcd for $C_{33}H_{50}O_3$: C, 80.11; H, 10.19; Found: C, 80.16; H, 10.52.

Alkyne compound 2a (PE/EA = 15:1): Yield: 93%. ^{1}H NMR (500 MHz, Chloroform-d) δ 5.27 (t, *J* = 3.8 Hz, 1H, H-13), 4.69 – 4.54 (m, 2H, H-32), 3.21 (dd, *J* = 11.1, 4.9 Hz, 1H, H-2), 2.41 (t, *J* = 2.5 Hz, 1H, H-18), 2.24 (dd, *J* = 11.1, 1.8 Hz, 1H), 2.02 (td, *J* = 13.3, 4.5 Hz, 1H), 1.91 (dd, *J* = 8.9, 3.7 Hz, 2H), 1.83 – 1.67 (m, 3H), 1.68 – 1.52 (m, 3H), 1.53 – 1.44 (m, 3H), 1.41 – 1.23 (m, 6H), 1.10 (dd, *J* = 4.8, 2.3 Hz, 1H), 1.08 (s, 3H), 0.99 (s, 3H), 0.94 (d, *J* = 6.3 Hz, 3H), 0.92 (s, 3H), 0.86 (d, *J* = 6.4 Hz, 3H), 0.77 (d, *J* = 6.8 Hz, 6H), 0.72 (dd, *J* = 11.7, 1.7 Hz, 1H). ^{13}C NMR (126 MHz, Chloroform-d) δ 176.64 (C=O), 137.77 (C=C), 125.88 (C=C), 79.04 (C≡C), 78.12 (C-OH), 74.38 (C≡C), 55.23 (C-O-), 52.83, 51.59, 48.19, 47.57, 42.06, 39.62, 39.08, 38.80, 38.76, 38.66, 36.98, 36.43, 33.07, 30.64, 29.70, 28.14, 28.03, 27.25, 23.50, 23.32, 21.16, 18.33, 17.20, 16.99, 15.62, 15.49. ESI-MS: Calcd for $C_{33}H_{50}O_3$, $[M]^+$: 494.38; Found: 495.33. Anal. Calcd for $C_{33}H_{50}O_3$: C, 80.11; H, 10.19; Found: C, 79.92; H, 10.22.

Alkyne compound 3a (PE/EA = 15:1): Yield: 87%. ^{1}H NMR (500 MHz, Chloroform-d) δ 5.71 (s, 1H, H-13), 4.82 – 4.63 (m, 2H, H-35), 3.25 (dt, *J* = 10.9, 5.3 Hz, 1H, H-2), 2.82 (dt, *J* = 13.5, 3.6 Hz, 1H, H-18), 2.49 (t, *J* = 2.4 Hz, 1H), 2.36 (s, 1H, H-10), 2.19 – 2.11 (m, 1H), 2.10 – 2.00 (m, 2H), 1.96 (ddd, *J* = 13.6, 4.3, 2.7 Hz, 1H), 1.85 (td, *J* = 13.7, 4.6 Hz, 1H), 1.74 – 1.61 (m, 3H), 1.59 (s, 9H), 1.53 – 1.39 (m, 3H), 1.39 (s, 4H), 1.38 – 1.25 (m, 2H), 1.20 (s, 3H), 1.16 (d, *J* = 5.3 Hz, 6H), 1.03 (s, 3H), 0.83 (d, *J* = 1.4 Hz, 6H), 0.72 (dd, *J* =

11.9, 1.9 Hz, 1H, H-4,). ^{13}C NMR (126 MHz, Chloroform-d) δ 200.21 (C=O), 175.60 (-COO), 168.95 (C=C), 128.62 (C=C), 77.01 (C≡C), 76.76 (C-OH), 74.74 (C≡C), 61.82, 54.96, 51.84, 48.20, 45.39, 43.96, 43.19, 41.07, 39.14, 37.60, 37.10, 32.78, 31.83, 31.15, 29.70, 28.43, 28.11, 28.04, 27.33, 26.49, 26.43, 23.38, 18.69, 17.50, 16.37, 15.58. Calcd for $C_{33}H_{48}O_4$, $[M]^+$: 508.36; Found: 509.58. Anal. Calcd for $C_{33}H_{48}O_4$: C, 77.91; H, 9.51; Found: C, 77.86; H, 9.73.

Alkyne compound 4a (PE/EA = 15:1): Yield: 89%. ^{1}H NMR (500 MHz, Chloroform-d) δ 5.30 (t, *J* = 3.7 Hz, 1H, H-13), 4.73 – 4.54 (m, 2H, H-32), 3.25 – 3.17 (m, 1H, H-2), 2.91 – 2.82 (m, 1H, H-18), 2.41 (t, *J* = 2.4 Hz, 1H, H-14), 2.06 – 1.91 (m, 1H, H-14), 1.87 (hd, *J* = 7.3, 3.7 Hz, 2H), 1.74 – 1.49 (m, 14H), 1.33 – 1.21 (m, 2H), 1.13 (s, 3H), 1.08 (dt, *J* = 14.0, 3.6 Hz, 1H), 0.98 (s, 3H), 0.92 (s, 3H), 0.90 (d, *J* = 2.7 Hz, 6H), 0.78 (s, 3H), 0.75 (s, 3H), 0.72 (dd, *J* = 11.7, 2.2 Hz, 1H, H-4). ^{13}C NMR (126 MHz, Chloroform-d) δ 176.84 (C=O), 143.40 (C=C), 122.62 (C=C), 79.02 (C≡C), 78.13 (C-OH), 74.38 (C≡C), 55.23 (C-O), 51.64, 47.63, 46.79, 45.85, 41.71, 41.30, 39.40, 38.76, 38.47, 37.04, 33.84, 33.08, 32.76, 32.20, 30.67, 28.11, 27.68, 27.21, 25.84, 23.62, 23.43, 23.03, 18.35, 17.10, 15.58, 15.35. ESI-MS: Calcd for $C_{33}H_{50}O_3$, $[M]^+$ 494.38; Found: 495.33. Anal. Calcd for $C_{33}H_{50}O_3$: C, 80.11; H, 10.19; Found: C, 79.17; H, 10.17.

The general synthesis of gold complexes 1b-4b: A 25 mL round bottomed flask was charged with **1a-4a** (0.0405 mmol) and THF (6 mL). NaHMDS (1.0 solution in THF) was added dropwise with vigorous stirring for 10 mins. Then Cl-Au-PPh_3 (0.0405 mmol) was added and the reaction was stirred for 4 h under the protection of nitrogen. Next, the reaction solution was concentrated in vacuo and the residue was further purified by column chromatography (Al_2O_3; PE/EA).

Gold(I) complex BA (1b) (PE/EA = 2:1): Yield: 84%. ^{1}HNMR (500 MHz, Chloroform-d) δ 7.55 – 7.46 (m, 9H, H-Ar), 7.48 – 7.40 (m, 6H, H-Ar), 4.89 –

4.76 (m, 2H, H-30), 4.75 – 4.55 (m, 2H, H-32), 3.16 (d, *J* = 10.6 Hz, 1H, H-2), 3.06 (td, *J* = 11.0, 4.5 Hz, 1H), 2.40 – 2.22 (m, 2H), 2.00 – 1.87 (m, 2H), 1.72 – 1.60 (m, 5H), 1.57 (s, 4H), 1.49 (td, *J* = 13.3, 12.7, 3.4 Hz, 2H), 1.45 – 1.29 (m, 5H), 1.14 (dt, *J* = 13.7, 3.3 Hz, 1H), 0.98 – 0.91 (m, 9H), 0.88 (t, *J* = 6.8 Hz, 5H), 0.71 (s, 3H), 0.67 (s, 3H), 0.63 (dd, *J* = 11.9, 2.0 Hz, 1H). ^{13}C NMR (126 MHz, Chloroform-d) δ 175.51 (C=O), 150.83 (C≡C), 134.30 (C=C), 134.19 (Ar-C), 131.60 (Ar-C), 129.90 (Ar-C), 129.20 (Ar-C), 129.11 (Ar-C), 109.40 (C=C), 78.99 (C≡C), 56.50 (C-OH), 55.33, 53.05 (C-OH), 50.63, 49.64, 46.83, 42.41, 40.00, 38.82, 38.14, 37.17, 36.83, 34.36, 32.07, 31.58, 30.65, 29.78, 29.69, 27.97, 27.42, 25.61, 22.64, 20.92, 19.42, 18.32, 16.56, 15.35, 14.70, 14.12. ESI-MS: Calcd for $C_{51}H_{64}AuO_3P$, $[M]^+$: 952.43, Found: 975.75. Anal. Calcd for $C_{51}H_{64}AuO_3P$: C, 64.28; H, 6.77; Found: C, 64.03; H, 6.98.

Gold(I) complex UA (2b) (PE/EA = 2:1): Yield: 74%. ^{1}HNMR (500 MHz, Chloroform-d) δ 7.53 (dd, *J* = 14.6, 6.3 Hz, 10H, Ar-H), 7.47 (d, *J* = 7.1 Hz, 5H, Ar-H), 5.31 (d, *J* = 3.9 Hz, 1H, H-13), 4.81 (s, 2H, H-32), 3.21 (dt, *J* = 10.5, 4.7 Hz, 1H, H-2), 2.31 (d, *J* = 11.3 Hz, 1H, H-18), 2.08 – 1.82 (m, 4H), 1.82 – 1.71 (m, 2H), 1.60 (d, *J* = 6.4 Hz, 4H), 1.31 (dt, *J* = 13.9, 8.7 Hz, 12H), 1.09 (s, 3H), 0.98 (s, 3H), 0.95 (d, *J* = 6.4 Hz, 2H), 0.91 (d, *J* = 6.3 Hz, 1H), 0.87 (d, *J* = 5.9 Hz, 6H), 0.83 (s, 3H, H-28), 0.73 (d, *J* = 8.7 Hz, 3H, H-29). ^{13}C NMR (126 MHz, Chloroform-d) δ 177.04 (C=O), 137.93 (C≡C), 134.32 (C=12), 131.59 (Ar-C), 129.89 (Ar-C), 129.45 (Ar-C), 129.20 (Ar-C), 129.11 (C=C), 125.73 (C≡C), 79.07 (C-OH), 55.22 (C-O-), 53.28, 52.73, 48.05, 47.65, 42.01, 39.63, 39.11, 38.76, 38.73, 38.61, 36.96, 36.37, 33.04, 31.60, 30.71, 28.13, 27.24, 24.14, 23.56, 23.36, 22.66, 21.23, 18.33, 17.40, 17.01, 15.62, 14.10. ESI-MS: Calcd for $C_{51}H_{64}AuO_3P$, $[M]^+$: 952.43. Found: 975.75. Anal. Calcd for $C_{51}H_{64}AuO_3P$: C,64.28; H,6.77; Found: C, 63.88; H, 6.94.

Gold(I) complex GA (3b) (PE/EA = 2:1): Yield: 76%. ^{1}H NMR (500 MHz, Chloroform-d) δ 7.58 – 7.42 (m, 15H, Ar-H), 5.80 (s, 1H, H-13), 4.88 (s, 2H, H-35), 3.29 – 3.19 (m, 1H, H-2), 2.80 (dt, *J* = 13.6, 3.8 Hz, 1H), 2.34 (s, 1H, H-18), 2.25 (dd, *J* = 13.5, 4.2 Hz, 1H, H-27), 2.12 – 1.95 (m, 3H), 1.83 (td, *J* =

13.8, 4.5 Hz, 1H), 1.45 – 1.33 (m, 6H), 1.29 (t, *J* = 5.9 Hz, 6H), 1.20 (s, 3H), 1.12 (d, *J* = 9.6 Hz, 6H), 1.02 (s, 4H), 0.90 (t, *J* = 6.7 Hz, 4H), 0.82 (d, *J* = 3.9 Hz, 6H), 0.71 (d, *J* = 11.7 Hz, 1H, H-4). ^{13}CNMR (126 MHz, Chloroform-d) δ 199.98 (-C=O), 176.02(-COO), 168.97 (C=C), 134.36 (C≡C), 131.53 (Ar-C), 131.51 (Ar-C), 129.91 (Ar-C), 129.47 (Ar-C), 129.17 (Ar-C), 129.08 (Ar-C), 128.67 (C=C), 78.81 (C≡C), 77.22 (C-OH), 61.73, 54.92 (C-O-), 53.66, 53.64, 47.90, 45.32, 43.90, 43.14, 41.14, 39.13, 39.10, 37.78, 32.77, 31.85, 31.59, 28.45, 28.14, 28.10, 27.33, 26.48, 23.38, 22.66, 18.68, 17.51, 16.37, 15.59, 14.13. ESI-MS: Calcd for $C_{51}H_{62}AuO_4P$, $[M]^+$: 966.99. Found: 989.75. Anal. Calcd for $C_{51}H_{62}AuO_4P$: C, 63.35; H, 6.46; Found: C, 63.64; H, 6.90.

Gold(I) complex OA (4b) (PE/EA = 2:1): Yield: 76%. ^{1}H NMR (500 MHz, Chloroform-d) δ 7.63 – 7.42 (m, 15H), 5.33 (t, *J* = 3.9 Hz, 1H, H-13), 4.83 (t, *J* = 2.1 Hz, 2H, H-34), 3.21 (dt, *J* = 10.5, 4.9 Hz, 1H, H-2), 2.91 (dd, *J* = 14.0, 4.5 Hz, 1H, H-18), 2.09 – 1.88 (m, 2H, H-14), 1.84 (ddd, *J* = 18.5, 6.6, 4.0 Hz, 1H), 1.77 – 1.38 (m, 8H), 1.31 (tdd, *J* = 13.9, 12.2, 9.9, 5.7 Hz, 8H), 1.24 – 1.14 (m, 2H), 1.14 (s, 3H, H-25), 0.97 (s, 3H, H-31), 0.92 (d, *J* = 11.2 Hz, 3H, H-28), 0.90 (s, 3H, H-30), 0.86 (s, 3H, H-27), 0.81 (s, 3H, H-26), 0.72 (s, 3H, H-29), 0.70 (s, 1H, H-4). ^{13}C NMR (126 MHz, Chloroform-d) δ 206.98 (C=O), 177.18 (C≡C), 143.71 (C=C), 134.29 (Ar-C), 134.18(Ar-C), 131.59 (Ar-C), 131.57 (Ar-C), 129.89 (Ar-C), 129.20 (Ar-C), 129.11 (Ar-C), 122.38 (C=C), 79.04 (C-OH), 55.21 (C-O-), 53.34, 47.70, 46.65, 45.96, 41.68, 41.31, 39.42, 38.72, 38.43, 37.02, 33.91, 33.15, 32.76, 32.13, 30.94, 30.70, 28.08, 27.83, 27.21, 25.88, 23.74, 23.45, 22.95, 18.34, 17.38, 15.56, 15.37. ESI-MS: Calcd for $C_{51}H_{64}AuO_3P$, $[M]^+$: 952.43; Found: 975.75. Anal. Calcd for $C_{51}H_{64}AuO_3P$: C, 64.28; H, 6.77; Found: C, 64.09; H, 7.10.

The general synthesis of cobalt complexes 1c-4c: A 25 mL round bottomed flask was charged with **1a-4a** (0.0405 mmol), cobaltcarbonyl (0.0585 mmol), THF (6 mL) and stirred for 16 h under room temperature. Then the reaction solution was concentrated in vacuo and the rude residue was further purified

by column chromatography (Al_2O_3; PE/EA).

Cobalt complex BA (1c) (PE/EA = 15:1): Yield: 89%. IR: 2016.45; 2054.57; 2096.34 cm^{-1}. ^1H NMR (500 MHz, Chloroform-*d*) δ 6.09 (s, 1H), 5.25 (s, 1H), 4.84 – 4.55 (m, 2H), 3.30 – 2.97 (m, 2H), 2.51 – 2.19 (m, 2H), 2.11 – 1.88 (m, 2H), 1.77 – 1.18 (m, 16H), 1.10 – 0.90 (m, 7H), 0.81 (d, *J* = 33.1 Hz, 4H), 0.74 – 0.63 (m, 1H). ^{13}C NMR (126 MHz, Chloroform-d) δ 199.16 (C=O), 150.45 (C=C), 109.66 (C=C), 88.57 (C≡C), 78.99 (C-OH), 72.32 (C≡C), 65.06 (C-OH), 56.73, 55.35, 50.57, 49.67, 46.85, 42.40, 40.69, 38.86, 38.72, 38.24, 37.21, 36.67, 34.34, 31.96, 31.70, 30.55, 27.98, 27.41, 25.52, 20.89, 19.39, 18.30, 16.14, 16.02, 15.36, 14.72. ESI-MS: Calcd for $C_{39}H_{50}Co_2O_9$, $[M]^+$: 780.21; Found: $[M\text{-}Co]^+$: 724.0.

Cobalt complex UA (2c) (PE/EA = 15:1): Yield: 68%. IR: 2022.60; 2056.82; 2096.06 cm^{-1}. ^1H NMR (500 MHz, Chloroform-*d*) δ 6.09 (s, 1H), 5.31 (s, 1H), 5.25 – 5.05 (m, 2H), 3.24 (d, *J* = 10.8 Hz, 1H), 2.49 – 2.19 (m, 2H), 1.41 – 1.25 (m, 14H), 1.11 (s, 5H), 1.03 – 0.93 (m, 7H), 0.93 – 0.85 (m, 7H), 0.76 (dd, *J* = 20.8, 12.2 Hz, 9H). ^{13}C NMR (126 MHz, Chloroform-d) δ 199.20 (C=O), 170.46 (C=C), 138.19 (C=C), 125.87 (-CO-), 125.73 (-CO-), 79.03 (C≡C), 74.39 (C-OH), 72.36 (C≡C), 55.20 (C-O-), 52.68, 51.59, 48.23, 47.52, 42.06, 41.98, 39.51, 39.04, 38.75, 36.96, 32.91, 31.93, 31.51, 30.61, 28.13, 28.07, 27.22, 23.99, 23.66, 23.25, 21.17, 18.31, 16.98, 16.96, 15.61, 15.37, 14.20. ESI-MS: Calcd for $C_{39}H_{50}Co_2O_9$, $[M]^+$: 780.21; Found: $[M\text{-}Co]^+$: 724.0.

Cobalt complex GA (3c) (PE/EA = 15:1): Yield: 56%. IR: 2024.42; 2056.68; 2096.45 cm^{-1}. ^1H NMR (500 MHz, Chloroform-*d*) δ 6.10 (s, 1H), 5.71 (s, 1H), 5.40 – 5.17 (m, 2H), 3.25 (dt, *J* = 11.0, 5.6 Hz, 1H), 2.82 (dt, *J* = 13.5, 3.6 Hz, 1H), 2.36 (s, 1H), 2.33 – 2.13 (m, 2H), 2.12 – 1.95 (m, 3H), 1.86 (td, *J* = 13.7, 4.6 Hz, 1H), 1.65 (td, *J* = 14.0, 5.5 Hz, 5H), 1.50 – 1.40 (m, 2H), 1.39 (s, 3H), 1.37 – 1.26 (m, 4H), 1.24 (s, 4H), 1.16 (d, *J* = 4.5 Hz, 6H), 1.09 – 0.95 (m, 5H), 0.84 (d, *J* = 8.4 Hz, 7H), 0.76 – 0.69 (m, 1H). ^{13}C NMR (126 MHz, Chloroform-d) δ 200.08 (C=O), 176.19 (-COO), 168.85 (C=C), 128.68 (C=C), 78.79 (C≡C), 72.31 (C-OH), 65.67 (C-O-), 61.81, 54.95 (C≡C), 48.17, 45.39, 44.17, 43.20, 41.11, 39.17, 39.15, 37.90, 37.09, 32.77, 31.89, 28.51, 27.32,

26.48, 23.44, 18.69, 17.50, 16.39, 15.58. ESI-MS: Calcd for $C_{39}H_{48}Co_2O_{10}$, $[M]^+$:795.25; Found: $[M]^+$: 795.25.

Cobalt complex OA (4c) (PE/EA = 15:1): Yield: 97%. IR: 2022.33; 2056.84; 2096.35cm^{-1}. ^{1}H NMR (500 MHz, Chloroform-*d*) δ 6.09 (s, 1H), 5.35 (d, *J* = 4.7 Hz, 1H), 5.28 – 5.09 (m, 2H), 3.23 (d, *J* = 10.7 Hz, 1H), 2.95 (dd, *J* = 13.7, 4.4 Hz, 1H), 2.08 – 1.97 (m, 1H), 1.94 – 1.86 (m, 2H), 1.76 – 1.53 (m, 8H), 1.51 – 1.40 (m, 1H), 1.34 – 1.24 (m, 5H), 1.16 (s, 3H), 1.01 (s, 4H), 0.91 (q, *J* = 6.6, 5.9 Hz, 12H), 0.77 (d, *J* = 23.6 Hz, 8H). ^{13}C NMR (126 MHz, Chloroform-d) δ 199.19 (C=O), 177.70 (C=C), 143.72 (C=C), 122.58 (-CO-), 88.50 (C≡C), 79.02 (C-OH), 72.42 (C≡C), 65.73 (C-O-), 55.21, 47.62, 46.91, 45.79, 41.65, 41.25, 39.30, 38.76, 38.40, 37.04, 33.81, 33.13, 32.64, 31.59, 30.66, 28.09, 27.80, 27.19, 26.01, 23.55, 22.80, 22.66, 18.33, 15.56, 15.23. ESI-MS: Calcd for $C_{39}H_{50}Co_2O_9$, $[M]^+$:780.21; Found: $[M\text{-}Co]^+$: 724.0; $[M\text{-}2Co+Na]^+$: 691.92.

Growth Inhibitory Assay

Cells were seeded into 96-well plates at a density of 2 × 10^3 per well and allowed to attach overnight in DMEM containing 10% heat-inactivated FBS. **4b** dissolved in DMF and the control group was treated with 0.1% DMF. The antiproliferative effect of compounds was measured using the MTT cytotoxicity assay. The specific steps are as follows: adding 5% MTT (5 mg/mL, PBS) reagent to the cells treated with the compounds, incubating for 4 h at 37 °C, 5% CO_2, then carefully discarding the culture medium, adding 200 μL DMSO and shaking on a shaker at a low speed about 10 min. Detected the absorbance at 490 nm. The concentration range of each complex was selected based on the cytotoxicity. The growth inhibitory rates of the complexes were calculated as ($OD_{control}$ − OD_{test}) / $OD_{control}$ × 100%. Half maximal inhibitory concentration (IC_{50}) value of the drug concentration corresponding to the inhibition rate at 50% was calculated using Graphpad Prism 5 statistical analysis. All experiments were conducted three times to

ensure the reproducibility of the results.

Purified TrxR Enzyme Assay

DMF or with **4b** (1.25 μM, 2.5 μM, 5 μM, 10 μM), OA (6.25 μM, 12.5 μM, 25 μM, 50 μM), auranofin (0.03125 μM, 0.0625 μM, 0.125 μM, 0.25 μM, 0.5μM) and rat liver TrxR (0.15 U) were dissolved in 50 μL reaction buffer. Added 225 μL of reaction mixture to each well. And the reaction was started by adding 25 μL solution of 20 mM DTNB. After appropriate mixing, record the absorption data at 405 nm with a microplate reader. The increase in TNB concentration over time follows a linear trend ($r^2 \geq 0.99$), and the enzyme activity is calculated as its slope (increased absorbance per thirty seconds). For each test compound, it was confirmed by non-interference test components by using a negative control experiment without an enzyme solution.

Quantitative Real-time Polymerase Chain Reaction

Trizol reagent was used to extract A2780 RNA according to the protocol. Real-time PCR was executed by 7500 RT-PCR system as described previously.[43] The mRNA levels of the target genes were calculated and results are from triplicate experiments. The following primers (GenScript, Nanjing, China) were used: β-actin: (forward) 5′-TGTGGATCAGCAAGCAGGAGTA-3′, (reverse) 5′-TGCGCAAGTTAGGTTTT GTCA-3′.

TrxR: (forward) 5′-GCCCTGCAAGACTCTCGAAATTA-3′,

(reverse) 5′-GCCCATAAGCATTCTCATAGACGA-3′.

Cellular Activities of TrxR Assay

When A2780 cells grew to an abundance of 70 - 80%, treated with different concentrations of **4b** for 24 h. Then, the culture was carefully discarded and washed twice with PBS. Total cell protein was extracted by treatment with RIPA buffer in an ice bath and quantified using the Bradford program. The activity of TrxR in cells was determined according to the TrxR activity detection kit (Beijing Solarbio Science & Technology).

Immunofluorescence Staining

A2780 cells were seeded in 24 - well plates and cultured for 24 h, then treated with **4b** for another 24 h. Incubating with antibodies overnight at 4 °C, followed by treating with anti-mouse or anti-rabbit IgG for 2 h and then the A2780 cells were washed with PBS for three times. The nuclei of A2780 cancer cells were dyed by 4′,6-Diamidino-2-phenylindole (DAPI). Immunofluorescence was detected with a fluorescence microscope (Leica DMi8).

Western Blot Analysis

A2780 cells (1×10^6 cells / well) were inoculated into a 10 cm diameter tissue culture dish (10 mL / well), and cultured at 37 °C, 5% CO_2 environment for 24 h, and then treated with **4b** at different dose for another 24 h, carefully discarded the medium, and washed with cold PBS, three times. Cell lysates were prepared using protease and phosphatase inhibitors. BCA assay kits were used to determine protein levels (Pierce, ThermoFisher Scientific, Waltham, MA, USA). After the separation process, the proteins were imprinted onto the PVDF membranes and blocked overnight in TBST (20 mM Tris-HCl, pH = 7.6, 0.1% v/v Tween-20), and incubated with the suitable secondary antibody for 2 h, then washed with TBST three times, the bands of protein detected by chemiluminescence procedure (ECL, Amersham).

10.1002/chem.202000045

Intracellular ROS Measurement and ROS-ERS Colocalization

A2780 cells (2×10^4 cells / well) were inoculated in 24-well plates and treated with **4b** incubated for 24 h, then washed with PBS and 10 μM CM-$DCFH_2$-DA for 20 min at 37 °C in darkness. ROS generation in A2780 cells was assessed by the fluorescent probe CM-$DCFH_2$-DA (Molecular Probes, Invitrogen). The ER-Tracker Red was used to examine the effects of binding to sulfonylurea receptors in the ER. The fluorescence increase was visualized by a Leica DMi8 fluorescent microscopy.

Measurement of MMP

A2780 cells (2×10^4 cells / mL) were seeded on cover slips in a 24-well plate and incubated for 24 h in supplemental medium and then treated with **4b** or DMF in 5% CO_2 culture conditions at 37 °C for 2 h. After that, the cells were treated with JC-1 (5 μM) for 30 min, washed with PBS buffer for three times, the cell staining was observed with a fluorescence microscope.

Cell Cycle Arrest and Apoptosis Analysis

A2780 cells (2×10^4 cells / well) were seeded in 6-well plates and cultured for 24 h followed by the treatment with DMF or **4b** for another 72 h. Cellular DNA flow cytometric kits (Nanjing Key Gen Biotech) were used according to the manufacturer's protocol to determine the stage of the cell cycle, specifically G0/G1, S, or G2/M, by flow cytometry (BD, Franklin Lakes, NJ, USA). Apoptosis was determined by FITC-labeled annexin V/PI double staining. The percentages of annexin-positive A2780 cells without PI staining were

determined by flow cytometry (FACS Calibur; BD). The data were analysed using cell quest software.

DNA Binding Test

The interaction of complex **4b** with CT-DNA was studied by UV-Vis in Tris · HCl buffer (5 mM Tris · HCl / 50 mM NaCl, pH 7.4), and CD in spectroscopy in PBS buffer (10 mM, pH = 7.2). The CT-DNA (1.24 mM) stock solution was stored in a refrigerator at 4 °C and stored for less than 5 days before use.

UV-Vis spectral Analysis

Complex **4b** stock solution was diluted 200 times with Tris · HCl buffer to obtain 1.0×10^5 M solution (3 mL). Then CT-DNA stock solution was added gradually. When the mixture solution had reacted sufficiently, the UV-Vis absorption spectra were recorded.

Circular Dichroism Spectral Analysis

Complex **4b** was dissolved in PBS buffer (10 mM, pH = 7.2). A series of samples containing ct-DNA (50 μM) and increasing concentrations of complex **4b** (r_b = [complex] / [DNA]), r_b = 0.0, 0.1, 1.0, 2.0) were prepared and incubated for 24 h at 37 °C. CD spectra were recorded in a cuvette of 1 cm path length, over the range of 200-500 nm, the scan rate of 200 nm·min^{-1} and the slit width of 3000 μm.

Electron Microscopy

10.1002/chem.202000045

A2780 cells were cultured in 6-well plates with the corresponding treatment. Then the cells were collected and fixed in phosphate buffer (pH 7.4) containing 2.5% glutaraldehyde overnight at 4 °C. The cells were post fixed in 1% OsO_4 at room temperature for 60 min, stained with 1% uranyl acetate, dehydrated through graded acetone solutions, and embedded in epon. Areas containing cells were block mount, cut into 70 nm sections and examined with the electron microscope. An Olympus EM208S transmission electron microscope was used to test.

Assessment of LDH Release

A2780 cells were cultured in 96-well plates with the corresponding treatment. LDH release was determined using commercially available kits according to the manufacturer's instructions (Jiancheng, China). Absorbance was measured at a wavelength of 450 nm. The data were expressed as a percentage of the control values. Each culture was performed in three duplicates.

Molecular Docking

The Schrödinger Maestro Software[44] was performed to predict and analyze the molecular docking of the component **4b** into the target protein TrxR (PDB: 3EAN).[38] The docking procedure was carried out by adding hydrogens, deleting waters, and setting the bond orders for crystal proteins and the radius of binding sites. The template Glide fitness score was set to evaluate the affinity. The possibility of the binding sites of **4b** was analyzed and validated according to the references.[5, 9a, 36-38]

Tumor Nude Mice Model

The mice were acclimated for 7 days after arrival before experiments started. A2780 cells (1.5×10^7 cells/mouse) were inoculated subcutaneously into the male Balb/c nude mice to create the cancer mouse models. After the tumor reached 180-200 mm^3, the mice were randomly divided into two groups (n = 5 or 6), and **4b** (20 mg/kg) or the same volume of normal saline was intraperitoneally injected every day, sustained 15 days, using a vernier caliper to measure the size of tumor every 2 days and calculate the tumor volume (TV) using the following formula: TV (mm^3) = $width^2$ (length / 2). The IRT were calculated as follows: IRT = 100% × $(M_1 – M_2)/M_1$; M_1 represents the mean weight of the tumor in the blank group and M_2 represents the mean weight of the tumor in the drug treatment group. All animal experiments were carried out upon approval of the Institutional Animal Care and Use Committee of Nanjing University of Chinese Medicine. All animals care was in accordance with institution guidelines. All efforts were made to minimize animal suffering during the experiments.

Acknowledgments

We thank the financial supports of the National Natural Science Foundation of China (No.81703337), the Priority Academic Program Development of Jiangsu Higher Education Institutions (Integration of Chinese and Western Medicine), the Jiangsu Specially-Appointed Professors program and the Open Project of State Key Laboratory of Natural Medicines (No. SKLNMKF201808, SKLNMKF201712), the State Key Laboratory of Coordination Chemistry, Nanjing University, the Six Talent Peaks Project in Jiangsu Province of China (No. SWYY-069).

Keywords: thioredoxin reductase · reactive oxygen species · endoplasmic reticulum stress · pentacyclic triterpene derivatives · gold complexes · ovarian cancer

References

[1] L. A. Torre, B. Trabert, C. E. DeSantis, K. D. Miller, G. Samimi, C. D. Runowicz, M. M. Gaudet, A. Jemal and R. L. Siegel, *CA Cancer J. Clin.* **2018**, *68*, 284-296.
[2] a) G. Jaouen, A. Vessieres and S. Top, *Chem. Soc. Rev.* **2015**, *44*, 8802-8817; b) Z. F. Chen, C. Orvig and H. Liang, *Curr. Top. Med. Chem.* **2017**, *17*, 3131-3145.
[3] H. Wu, R. Li, Z. Zhang, H. Jiang, H. Ma, C. Yuan, C. Sun, Y. Li and B. Kong, *J. Ovarian Res.* **2019**, *12*, 125.
[4] X. Li, Y. Hou, X. Meng, C. Ge, H. Ma, J. Li and J. Fang, *Angew. Chem. Int. Ed. Engl.* **2018**, *57*, 6141-6145.
[5] J. Zhang, B. Zhang, X. Li, X. Han, R. Liu and J. Fang, *Med. Res. Rev.* **2019**, *39*, 5-39.
[6] S. E. Eriksson, S. Prast-Nielsen, E. Flaberg, L. Szekely and E. S. Arner, *Free Radic. Biol. Med.* **2009**, *47*, 1661-1671.
[7] a) K. Wang, C. Zhu, Y. He, Z. Zhang, W. Zhou, N. Muhammad, Y. Guo, X. Wang and Z. Guo, *Angew. Chem. Int. Ed. Engl.* **2019**, *58*, 4638-4643; b) D. S. Alberts, P. T. Fanta, K. L. Running, L. P. Adair, Jr., D. J. Garcia, R. Liu-Stevens and S. E. Salmon, *Cancer Chemother. Pharmacol.* **1997**, *39*, 493-497; c) R. Fan, M. Bian, L. Hu and W. Liu, *Eur. J. Med. Chem.* **2019**, *183*, 111721.
[8] S. J. Welsh, W. T. Bellamy, M. M. Briehl and G. Powis, *Cancer Res.* **2002**, *62*, 5089-5095.
[9] a) J. Zhang, X. Li, X. Han, R. Liu and J. Fang, *Trends Pharmacol. Sci.* **2017**, *38*, 794-808; b) O. Rackham, A. M. Shearwood, R. Thyer, E. McNamara, S. M. Davies, B. A. Callus, A. Miranda-Vizuete, S. J. Berners-Price, Q. Cheng, E. S. Arner and A. Filipovska, *Free Radic. Biol. Med.* **2011**, *50*, 689-699.
[10] M. Bian, R. Fan, S. Zhao and W. Liu, *J. Med. Chem.* **2019**, *62*, 7309-7321.
[11] X. Chen, L. Song, Y. Hou and F. Li, *Oncol. Rep.* **2019**, *41*, 765-778.
[12] H. N. Gil, E. Jung, D. Koh, Y. Lim, Y. H. Lee and S. Y. Shin, *Chem. Biol. Interact.* **2019**, *298*, 72-79.
[13] a) L. Cui, W. Bu, J. Song, L. Feng, T. Xu, D. Liu, W. Ding, J. Wang, C. Li, B. Ma, Y. Luo, Z. Jiang, C. Wang, J. Chen, J. Hou, H. Yan, L. Yang and X. Jia, *Arch. Pharm. Res.* **2018**, *41*, 299-313; b) E. Hocsak, V. Szabo, N. Kalman, C. Antus, A. Cseh, K. Sumegi, K. Eros, Z. Hegedus, F. Gallyas, Jr., B. Sumegi and B. Racz, *Free Radic. Biol. Med.* **2017**, *108*, 770-784.
[14] a) H. Xie, X. Li, Y. Chen, M. Lang, Z. Shen and L. Shi, *J. Ethnopharmacol.* **2019**, *231*, 230-240; b) J. Zhu, S. Tian, K. T. Li, Q. Chen, Y. Jiang, H. D. Lin, L. H. Yu and D. Q. Bai, *Cancer Med.* **2018**, *7*, 1908-1920.
[15] a) G. X. Hou, P. P. Liu, S. Zhang, M. Yang, J. Liao, J. Yang, Y. Hu, W. Q. Jiang, S. Wen and P. Huang, *Cell Death Dis.* **2018**, *9*, 89; b) T. Zou, C. T. Lum, C. N. Lok, J. J. Zhang and C. M. Che, *Chem. Soc. Rev.* **2015**, *44*, 8786-8801.

[16] a) A. Casini, R. W. Sun and I. Ott, *Met. Ions. Life. Sci.* **2018**, *18*; b) S. Nobili, E. Mini, I. Landini, C. Gabbiani, A. Casini and L. Messori, *Med. Res. Rev.* **2010**, *30*, 550-580; c) S. J. Berners-Price and A. Filipovska, *Metallomics* **2011**, *3*, 863-873.
[17] I. Ott, X. Qian, Y. Xu, D. H. Vlecken, I. J. Marques, D. Kubutat, J. Will, W. S. Sheldrick, P. Jesse, A. Prokop and C. P. Bagowski, *J. Med. Chem.* **2009**, *52*, 763-770.
[18] E. Vergara, A. Casini, F. Sorrentino, O. Zava, E. Cerrada, M. P. Rigobello, A. Bindoli, M. Laguna and P. J. Dyson, *ChemMedChem.* **2010**, *5*, 96-102.
[19] J. Lu, C. Berndt and A. Holmgren, *Biochim. Biophys. Acta.* **2009**, *1790*, 1513-1519.
[20] a) H. Fan, L. Geng, F. Yang, X. Dong, D. He and Y. Zhang, *Eur. J. Med. Chem.* **2019**, *176*, 61-67; b) J. Wu, C. Yang, C. Guo, X. Li, N. Yang, L. Zhao, H. Hang, S. Liu, P. Chu, Z. Sun, B. Sun, Y. Lin, J. Peng, G. Han, S. Wang and Z. Tang, *Chem. Biol. Interact.* **2016**, *244*, 94-104.
[21] A. Meyer, C. P. Bagowski, M. Kokoschka, M. Stefanopoulou, H. Alborzinia, S. Can, D. H. Vlecken, W. S. Sheldrick, S. Wolfl and I. Ott, *Angew. Chem. Int. Ed. Engl.* **2012**, *51*, 8895-8899.
[22] A. Casini, R. W. Sun and I. Ott, *Met. Ions. Life Sci.* **2018**, *18*.
[23] a) X. Li, B. Zhang, C. Yan, J. Li, S. Wang, X. Wei, X. Jiang, P. Zhou and J. Fang, *Nat. Commun.* **2019**, *10*, 4360-4372; b) J. Yao, D. Duan, Z. L. Song, J. Zhang and J. Fang, *Free Radic. Biol. Med.* **2020**, doi. 10.1016/j.freeradbiomed.2020.1001.1008; c) B. Zhang, D. Duan, C. Ge, J. Yao, Y. Liu, X. Li and J. Fang, *J. Med. Chem.* **2015**, *58*, 1795-1805; d) D. Duan, B. Zhang, J. Yao, Y. Liu, J. Sun, C. Ge, S. Peng and J. Fang, *Free Radical Biol. Med.* **2014**, *69*, 15-25; e) D. Duan, B. Zhang, J. Yao, Y. Liu and J. Fang, *Free Radic Biol. Med.* **2014**, *70*, 182-193; f) R. Liu, D. Shi, J. Zhang, X. Li, X. Han, X. Yao and J. Fang, *Mol. Pharmaceutics* **2018**, *15*, 3285-3296; g) D. Duan, J. Zhang, J. Yao, Y. Liu and J. Fang, *J. Biol. Chem.* **2016**, *291*, 10021-10031.
[24] J. A. Lessa, J. C. Guerra, L. F. de Miranda, C. F. Romeiro, J. G. Da Silva, I. C. Mendes, N. L. Speziali, E. M. Souza-Fagundes and H. Beraldo, *J. Inorg. Biochem.* **2011**, *105*, 1729-1739.
[25] C. M. Chan, D. Y. Huang, Y. P. Huang, S. H. Hsu, L. Y. Kang, C. M. Shen and W. W. Lin, *J. Cell Mol. Med.* **2016**, *20*, 1749-1760.
[26] P. Kritsiligkou, J. D. Rand, A. J. Weids, X. Wang, C. J. Kershaw and C. M. Grant, *J. Biol. Chem.* **2018**, *293*, 11984-11995.
[27] S. Shen, Y. Zhang, R. Zhang, X. Tu and X. Gong, *Chem Biol Interact* **2014**, *218*, 28-41.
[28] W. Huang, Y. Liu, J. Wang, X. Yuan, H. W. Jin, L. R. Zhang, J. T. Zhang, Z. M. Liu and J. R. Cui, *Eur. J. Med. Chem.* **2018**, *157*, 887-897.
[29] F. Y. Wang, K. B. Huang, H. W. Feng, Z. F. Chen, Y. N. Liu and H. Liang, *Free Radic. Biol. Med.* **2018**, *129*, 418-429.
[30] J. Y. Sun, Y. J. Hou, X. Y. Fu, X. T. Fu, J. K. Ma, M. F. Yang, B. L. Sun, C. D. Fan and J. Oh, *Front. Physiol.* **2018**, *9*, 1907.
[31] Y. Li, Q. Wu, G. Yu, L. Li, X. Zhao, X. Huang and W. Mei, *Eur. J. Med. Chem.* **2019**, *164*, 282-291.
[32] a) S. Gu, C. Chen, X. Jiang and Z. Zhang, *Chem. Biol. Interact.* **2016**, *245*, 100-109; b) K. B. Huang, F. Y. Wang, X. M. Tang, H. W. Feng, Z. F. Chen, Y. C. Liu, Y. N. Liu and H. Liang, *J. Med. Chem* **2018**, *61*, 3478-3490.
[33] a) L. J. Li, Y. Chai, X. J. Guo, S. L. Chu and L. S. Zhang, *Mol. Med. Rep.* **2018**, *17*, 7886-7892; b) J. J. Zhang, R. W. Sun and C. M. Che, *Chem. Commun. (Camb)* **2012**, *48*,

3388-3390.
[34] S. Jayakumar, R. S. Patwardhan, D. Pal, B. Singh, D. Sharma, V. K. Kutala and S. K. Sandur, *Free Radic. Biol. Med.* **2017**, *113*, 530-538.
[35] G. Jia, Q. Wang, R. Wang, D. Deng, L. Xue, N. Shao, Y. Zhang, X. Xia, F. Zhi and Y. Yang, *Onco. Targets Ther.* **2015**, *8*, 303-311.
[36] B. Zhang, J. Zhang, S. Peng, R. Liu, X. Li, Y. Hou, X. Han and J. Fang, *Expert. Opin. Ther. Pat.* **2017**, *27*, 547-556.
[37] D. Parsonage, F. Sheng, K. Hirata, A. Debnath, J. H. McKerrow, S. L. Reed, R. Abagyan, L. B. Poole and L. M. Podust, *J. Struct. Biol.* **2016**, *194*, 180-190.
[38] T. Zhang, P. Zheng, X. Shen, R. Shao, B. Wang, H. Shen, J. Zhang, Y. Xia and P. Zou, *Free Radic. Biol. Med.* **2019**, *141*, 93-102.
[39] a) C. M. Almeida, G. P. Nascimento, K. G. Magalhães, B. A. Iglesias and C. C. Gatto, *J. Coord. Chem.* **2018**, *71*, 502-519; b) A. Meyer, L. Oehninger, Y. Geldmacher, H. Alborzinia, S. Wolfl, W. S. Sheldrick and I. Ott, *ChemMedChem* **2014**, *9*, 1794-1800.
[40] a) X. Wu, X. Li, Z. Li, Y. Yu, Q. You and X. Zhang, *J. Med. Chem.* **2018**, *61*, 11280-11297; b) Z. Yu, W. Pan, N. Li and B. Tang, *Chem. Sci.* **2016**, *7*, 4237-4244.
[41] K. Li, Q. Zheng, X. Chen, Y. Wang, D. Wang and J. Wang, *Oxid. Med. Cell Longev.* **2018**, *2018*, 1915828.
[42] H. Lei, G. Wang, J. Zhang and Q. Han, *Oncol. Rep.* **2018**, *40*, 3447-3457.
[43] M. Bian, X. Chen, C. Zhang, H. Jin, F. Wang, J. Shao, A. Chen, F. Zhang and S. Zheng, *Biofactors* **2017**, *43*, 836-846.
[44] Z. Xu, K. Li, T. Pan, J. Liu, B. Li, C. Li, S. Wang, Y. Diao and X. Liu, *J. Ethnopharmacol.* **2019**, *239*, 111909.